SLD PHYSICS NOTE ????
Feburary 28, 2005
Draft 3.1

Measurement of the branching ratio of the Z^0 into heavy quarks

Nicolo de Groot, Su Dong, Thomas Wright, Sean Walston

ABSTRACT

We measure the hadronic branching ratios of the Z^0 boson into heavy quarks: $R_b = \Gamma_{Z^o \to b\bar{b}}/\Gamma_{Z^0 \to hadrons}$ and $R_c = \Gamma_{Z^o \to c\bar{c}}/\Gamma_{Z^0 \to hadrons}$ using a multi-tag technique. The measurement was performed using about 400,000 hadronic Z^0 events recorded in the SLD experiment at SLAC between 1996 and 1998. The small and stable SLC beam spot and the CCD-based vertex detector were used to reconstruct bottom and charm hadron decay vertices with high efficiency and purity, which enables us to measure most efficiencies from data. We obtain,

$$R_b = 0.21610 \pm 0.00098(stat.) \pm 0.00073(syst.) \mp 0.00012(R_c)$$

and,

$$R_c = 0.1745 \pm 0.0031(stat.) \pm 0.0020(syst.) \mp 0.0006(R_b)$$

1 Introduction

The dominant production of Z^0 decays, with large statistics, at e^+e^- experiments operating on the Z^0 peak, provides a unique opportunity for probing electroweak interactions at high precision. The democratic production of all fermion flavors in Z^0 decays with a clean initial state allows particularly sensitive tests of the Standard Model (SM) through measurements of $R_b = \Gamma_{Z^o \to b\overline{b}}/\Gamma_{Z^0 \to hadrons}$ and $R_c = \Gamma_{Z^o \to c\overline{c}}/\Gamma_{Z^0 \to hadrons}$, the heavy quark production fractions in hadronic Z^0 decays. The b and c quarks are the heaviest charge 1/3 and charge 2/3 quarks, respectively, that are accessible at the Z^0 energy. The R_b measurement has been traditionally a focus of attention as it is not only sensitive to the heavy top quark mass, but also widely regarded as a promising window for detecting new physics through radiative corrections to the $Z^0 \to b\overline{b}$ coupling. More generally, any unexpected difference in quark coupling of one flavor compared with other flavors could be a vital clue toward a solution to the puzzle of fermion family degeneracy.

To take full advantage of the large Z^0 decay samples as an effective flavor physics arena, the advance in vertex detector technologies has played a key role for flavor identification. Unprecedented performance in b quark tagging has made it possible to achieve R_b measurements [1][2] at below 1% precision. Our previous R_b measurement [2] has demonstrated the effectiveness of the combination of high resolution vertexing and the small and stable interaction point at the SLC, which pointed the way for very high purity b-tags and led to the reduction of systematic uncertainties for R_b measurements in general. In this paper we present an updated R_b measurement from SLD using $\sim$2.5 times more statistics than our previous publication and with an upgraded CCD pixel vertex detector, which improves the b-tag efficiency to approximately a factor of two higher than b-tags used in existing measurements at similar b-purity.

The existing measurements of the charm branching ratio R_c [3] are considerably less precise than the R_b measurements. These determinations of R_c rely on a number of methods to identify charm jets that all have certain disadvantages. Exclusive reconstruction of charmed mesons suffers from a small branching fraction and introduces a dependence on the actual value of this branching fraction and on the production fractions of the charm hadrons. Inclusive reconstruction using leptons or slow pions suffer from low purities and again a dependence on branching fractions. Due to the superb performance of the SLD vertex detector we are able to introduce an inclusive charm tag, based on lifetime information in a similar way as the b tag, which combines high efficiency with good purity. Moreover, the tagging efficiencies are measured from data and result in a minimal reliance on Monte Carlo simulation and a small systematic uncertainty. This leads to a new determination of R_c with much improved overall precision than the existing measurements.

Here is a summary of the updates since the last release at 2001 which led to these final R_b, R_c results for the PRD. The R_b measurement only evolved slightly from 2000 Osaka ICHEP, while R_c took a major upgrade to multi-tags in Winter 2001 and the last release before 2004 was summer 2001 with only minor polishing to both R_b and R_c. For the final 2004 update, although there are no major analysis method changes and majority of the physics systematics remain the same as summer 2001, but many several key systematics are

reexamined and updated. We released an updated result for summer 2004, considered as final, but the process of drafting the PRD brough a few more small changes. Here is a list of updates made at summer 2004:

- Analyses ntuples rerun with latest tracking resolution (Aaron's triplet based) corrections and all MC samples utilized including $c\overline{c}$ only MC.

- Default MC is now with both tracking resolution and efficiency correction. Previous analysis used only resolution correction and tracking efficiency was not appplied by default and only used as variation for systematics. We were previously not sure the apparent tracking efficiency correction needed to make data and MC track multiplicity agree a real efficiency issue or generator over production. The b, c vertex charge distributions finally broke the ambiguity to clearly implying there is real tracking inefficiency to be corrected.

- Gluon splitting effect reevaluated and uncovered an extra correction. The gluon splitting recommended by LEPEWWP based on measurements are $\sim \times 2$ higher than JETSET MC. We previously only corrected the $g \to Q\overline{Q}$ effect on uds efficiency. It turns out the $g \to Q\overline{Q}$ effect on $c\overline{c}$ efficiency is also significant, and there is also a slight effect on the correlations. The $g \to Q\overline{Q}$ scaling is now applied to all efficiencies and correlations.

- Extensive checks are made on b, c tag hemisphere correlations and reasonably good agreement found between component sums and MC total correlations. Various effects of the tag behavior previously unnoticed are observed. Systematic effects for two b's in same hemisphere reexamined.

- Detector systematic was previous using half of resolution correction and the full tracking eff correction as variations. Given that we are more confident about the origin of the track efficiency correction, its error is now also half the correction. However, there are two ways of estimating the systematics depending on the combination of tracking efficiency and resolution. We take the larger of the two estimates then divide by 2.

- IP tail effect reexamined with YT distributions and concluded no visible beam spot tail for 97-98, but 96 is consistent with having 0.5% tail at $100\,\mu$m. This systematics is added for 96.

- Our charm MC is slightly different in some respect compared to the LEPEWWG central values. This was previously uncorrected and only the variations was looked at for systematics. The R_b central value is now corrected for two of the most significant effects: $c\overline{c}$ hadron production spiecies (our MC had a bit more c-baryon) and D decay multiplicity (our MC D^+ 1-prong fraction low).

The additional updates for the PRD draft:

- Event selection bias reevaluated using all R17 MC samples for both R_b and R_c. The basic hadronic selection bias changed slightly, consistent with MC statistics compared to before. The 4-jet cut is reevaluated completely for version 3 of the PRD draft after realizing a problem in the JETSET 7.4 gluon radiation from heavy quarks following an E-mail exchange with Sjöstrand. Central values changed slightly from these updates.

- b correlation component study further updated to include ϕ and time correlations effects. Systematic errors due to time dependence and ϕ added, ϕ systematics also reevaluated. Half the discrepancy between the component sum and overall MC correlation from the 97-8 analysis is taken as an additional systematic error.

- b QCD hemisphere correlation reestimated using the correlation component study.

- c-tag correaltion are symmetrically studied as for the b-tag for θ, ϕ,time and QCD hemisphere correlation systematics.

- R_b (R_c) result rescaled to use exactly SM R_c (R_b) value.

2 Apparatus and Hadronic Event Selection

This analysis is based on approximately 400,000 hadronic events produced in e^+e^- annihilations at a mean center-of-mass energy of $\sqrt{s} = 91.28$ GeV at the SLAC Linear Collider (SLC), and recorded in the SLC Large Detector (SLD) between 1996 and 1998. A general description of the SLD can be found elsewhere [4]. The trigger and initial selection criteria for hadronic Z^0 decays are described in Ref. [5]. The Central Drift Chamber (CDC) [6] and the upgraded Vertex Detector (VXD3) [7], inside a uniform axial magnetic field of 0.6T, provide the momentum measurements of charged tracks and precision vertex information near the interaction point (IP), which are central to this analysis. The energies of clusters measured in the Liquid Argon Calorimeter [8] are used for event selection and calculation of the event thrust axis.

SLD uses a coordinate system with the z-axis parallel to the beam direction and x and y respectively are the horizontal and vertical coordinates perpendicular to the z-axis. The polar angle θ is measured with respect to the z-axis and the azimuthal angle ϕ is the angle with the x-axis in the xy plane.

The CDC and VXD3 give a combined momentum resolution of $\sigma_{p_\perp}/p_\perp = 0.01 \oplus 0.0026 p_\perp$, where $p_\perp$ is the track momentum transverse to the beam axis in GeV/c. The VXD3 consists of 3 barrels of Charged Coupled Devices (CCD) at radii of 2.7, 3.8 and 4.8 centimeters from the beam line, with 3-hit solid angle coverage up to $|\cos\theta|$=0.85. The CCD pixels are cubic active volumes of 20 μm on each side, which provide precise 3D spatial hits. This high granularity in 3D space enable our track finding algorithm to limit the hit mis-assignment rate to only 0.2%. The spatial resolution on the hit cluster centroid achieved after a track based CCD alignment [9] is $\sim$4 μm in both azimuthal and z directions. The resultant tracking resolution for high momentum tracks, as measured from the miss distances of two tracks near the IP in $Z^0 \to \mu^+\mu^-$ events, is 7.7 μm in $r\phi$ and 9.6 μm in rz. The multiple scattering

contribution to the track impact parameter resolution can be approximately expressed as $\frac{33}{p\sin^{3/2}\theta}$ μm. These numbers are roughly a factor of two better than a typical vertex detector at LEP. This resolution advantage combined with the small and stable SLC IP information is crucial in establishing the feasibility of the measurement techniques, in particular for the case of the inclusive charm tagging for the R_c measurement.

For the purpose of estimating the efficiencies and purities of the event selection and flavor tagging procedures, we use a detailed Monte Carlo (MC) simulation of the detector. The JETSET 7.4 [10] event generator is used, with parameter values tuned to hadronic e^+e^- annihilation data [11], combined with a simulation of the SLD based on GEANT 3.21 [12]. The simulations of heavy hadron production and charm decays are described in [5]. The B decay simulation is adapted from the CLEO QQ MC with additional tuning by SLD (see appendix B of [13]) to match a wider range of $\Upsilon(4S)$ B decay data.

For the hadronic event selection, we use a set of well-measured tracks, consistent with originating from within the beam pipe radius of 2.5 cm. The selected events have at least 7 tracks with $p_\perp$ >0.2 GeV/c and within 5 cm from the interaction point along the beam axis. There are at least 3 tracks with two or more VXD hits. The event visible energy E_{vis}, calculated from charged tracks with the charged pion mass assigned, must be at least 18 GeV. To ensure the events are well contained within the detector fiducial volume, we require the thrust-axis polar angle w.r.t. the beamline, θ_T, calculated using calorimeter clusters, to be within $|\cos\theta_T|$ <0.7. We only include events with $\leq$3 jets for the analysis, where the jets are reconstructed from tracks using the JADE algorithm [14] with $y_{cut} = 0.02$. This last requirement is to reject higher jet multiplicity events where the division of events into two hemispheres is no longer reliable for partitioning the events with one heavy hadron in each hemisphere.

The selected event sample contains 191,770 events from the 1997-98 runs and 29,996 events from the 1996 run. We analyze the two data samples separately because the small 1996 sample, recorded during the early VXD3 commissioning period, has a lower overall VXD hit efficiency due to electronics problems and some radiation damage. This effect was not present in the 97-98 period when the VXD3 ran at ∼10 degrees colder and the operation of the electronics was much more stable.

The estimated background in the hadronic event sample is negligible. The Monte Carlo $Z^0 \to hadrons$ event statistics used in the analysis have MC:data event ratios of 4:1, 15:1, and 22:1 for light flavor quarks (uds), $c\bar{c}$, and $b\bar{b}$ events, respectively.

To be clearer for internal reference, here are some specific details on the SLD analysis utilities used. The hadronic event selection is `BBESEL` as coded inside `B3MASS`. The CDC track and VXD track counting required `swmstat=0`. The important switches:

```
bbmkdtp.trkkalt   =  F  Use KAL thrust axis.
bbeselp.checkeit  =  T  Check EIT-1 result (as for data pass1).
bbeselp.checktkr  =  T  Avoid CDC layer 0,1 trip events.
bbeselp.checkvet  =  F  PHTRIG veto sim problem.  Don't use.
bbeselp.usecurph  =  F  Don't use stored PHCLASS. Recalculate.
```

Note that `BBESEL` also makes check through `VXRUNOK` to reject bad VXD run periods. In the analysis, data and MC events are both required to pass at least one of the following triggers:

TRACK,HADRON,WAB,MUON. For hadronic events passed all other selections, this trigger check rejects 0.2% of data and 0.1% hadronic MC and no flavor dependence in the MC loss.

Since the event counts has been a very effective check historically for spotting event selection inconsistencies in analyses, we also include a detailed table of the data and MC event counts. Both data and MC are from the R17 processing. The 'HAD' data is in fact all Z^0 decays including lepton pair events. We unfortunately didn't record the exact

Sample	All inputs	BBESEL skim	$\lvert\cos\theta_{thrust}\rvert < 0.7$	N_{jet}=2,3	Trigger
1997-98 samples					
Data	555541	250233	211581	192189	191770
MC all flavors	1572513	1090886	920105	845382	844538
uds		666923	561881	515578	515066
c		187368	158110	144792	144642
b		236595	200114	185012	184830
MC $b\overline{b}$	1577784	1097279	927289	856403	855526
MC $c\overline{c}$	933372	649098	547211	501954	501468
1996 samples					
Data	102699	39042	33105	30122	29996
MC all flavors	260948	179810	151911	139861	139732
uds		109964	92976	85358	85277
c		30745	25868	23790	23776
b		39101	33067	30713	30679
MC $b\overline{b}$	262992	181911	153780	142211	142062
MC $c\overline{c}$	155591	107699	90788	83454	83377

Table 1: Event sample statistics. The BBESEL event selection skim used $\lvert\cos\theta_{thrust}\rvert < 0.8$.

initial flavor composition for all flavor MC. However, care still needs to be taken even if they are available for evaluating the event selection flavor bias. The MC production had some crashed jobs and in principle that can conspire with bad VXD/CDC periods to make false flavor bias when comparing all flavor MC and $b\overline{b}$,$c\overline{c}$ only MC. The event selection bias evaluation is therefore based on all favor MC only and the input $uds/c/b$ fractions are taken from the Winter 2001 study using only all flavor MC.

The data and MC run period matching for the selected events and the b-tag fraction are shown in Fig. 1 for 97-8 and Fig. 2 for 96. The random trigger samples are not exactly matching the luminosity, as the random event skimming was done at the first processing which missed some runs which didn't show up in that processing and added later in the reprocessings. The all flavor and $b\overline{b}$ samples have a relatively complete collection of all jobs, but the $c\overline{c}$ samples are missing a few small preiods most likely due to crashed MC jobs not rerun with skipping bad events. The only significant time variation effect is in the 96 data where the middle period has the best performance, while the start and end of 96 had more dead channels due to the early electronics problems.

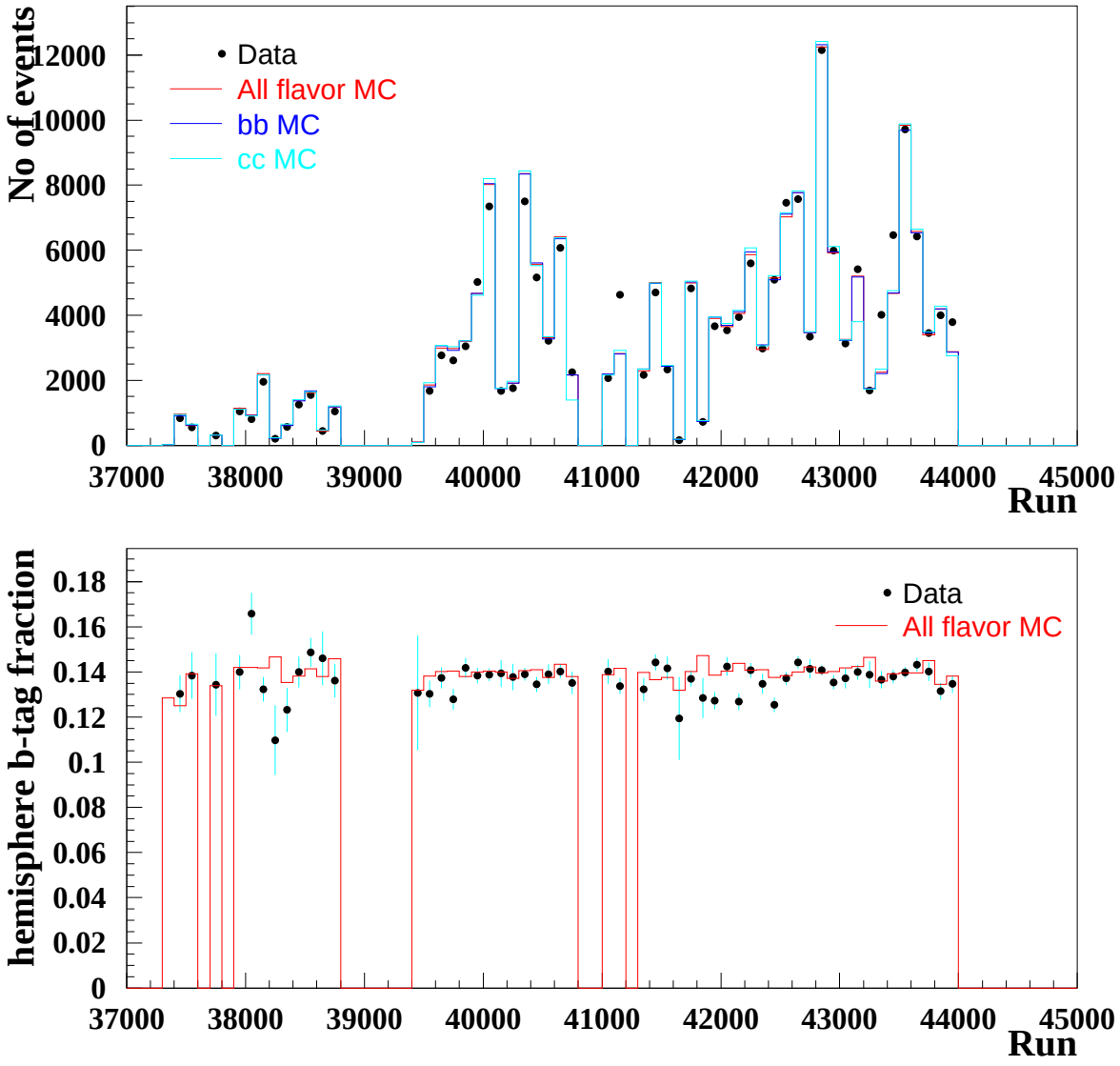

Figure 1: Data and MC sample time dependence comparison for 97-98.

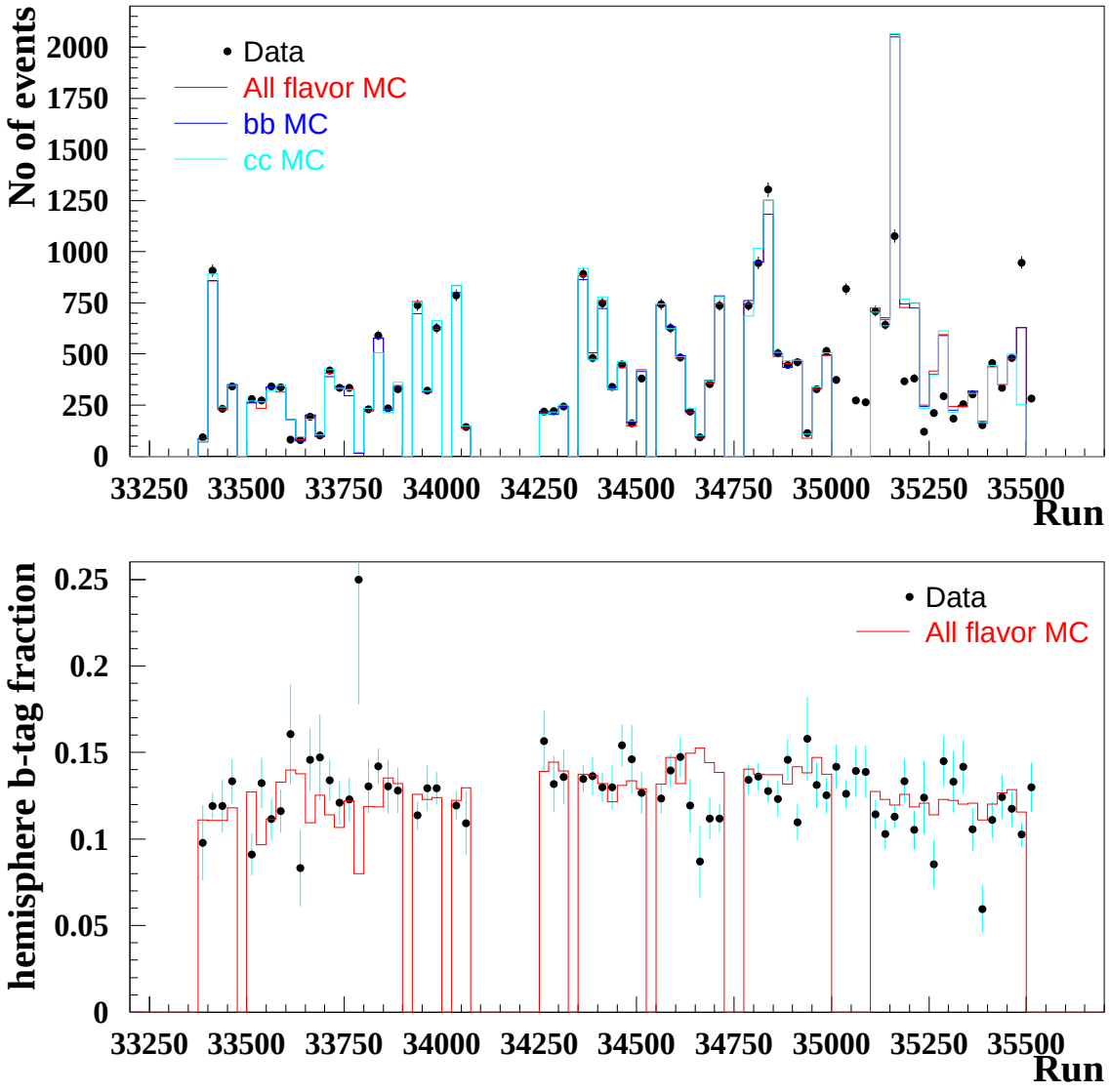

Figure 2: Data and MC sample time dependence comparison for 96.

3 Heavy Flavor Tagging

Decays of Z^0 bosons into charm and bottom quarks can be distinguished from those into light flavors (u,d and s) by searching for the heavy hadron decay vertices displaced from the event interaction point (IP). Because they are produced with high energy and have long lifetimes, heavy hadrons generally travel distances of millimeters before decaying. In a jet from a light quark the tracks will appear to come from one point in space, the event IP. In a charm jet some of the tracks may not point back to the IP, and if the charmed hadron decays into more than one charged particle there will be a secondary vertex (SV) in addition to the IP. Bottom jets will also exhibit secondary vertices, and if there are sufficient particles produced at the b and c decay points it is possible to find more than one displaced vertex. The reconstructed secondary vertices and their associated kinematic properties serve as the primary basis for flavor tagging for both $b\overline{b}$ and $c\overline{c}$ events in this analysis.

3.1 IP Reconstruction

To search for displaced vertices the position of the IP must be precisely known. In each event the position of the IP in the plane transverse to the beam axis is determined by fitting all tracks that are compatible with coming from the IP to a common vertex. Because the SLC luminous region is small and stable in the xy plane, sets of 30 time sequential hadronic events are averaged to obtain a more precise determination of the xy IP position (details in appendix A of [13]). The xy IP resolution is measured from the impact parameter distributions of $Z^0 \to \mu^+\mu^-$ events, deconvolved from the track impact parameter resolution measured from the two track miss distance, to obtain an IP resolution of $3.2\,\mu$m.

Because the SLC luminous region is larger in z ($700\ \mu$m), the z position of the IP must be found event-by-event. Tracks with VXD hits are extrapolated to their point of closest approach (POCA) in xy to the precisely determined transverse IP position. Tracks with impact parameters of more than $500\,\mu$m or 3 times the error (σ) from the IP are excluded, and the z position of the IP is taken from the median z at POCA of the remaining tracks. The resolution of this method is found from the Monte Carlo simulation to be $10/11/17\ \mu$m for $uds/c\overline{c}/b\overline{b}$ events.

3.2 Secondary Vertex Reconstruction

Secondary vertices are found using a topological algorithm [15]. This method searches for space points of large track density in 3 dimensions. Each track is parameterized by a Gaussian probability density tube $f(\vec{r})$ with a width equal to the uncertainty in the track position at its POCA to the IP, $\vec{r}_0$:

$$f(\vec{r}) = \exp\left\{-\frac{1}{2}\left[\left(\frac{x-(x_0+y^2\kappa)}{\sigma_1}\right)^2 + \left(\frac{z-(z_0+y\tan\lambda)}{\sigma_2}\right)^2\right]\right\}. \qquad (1)$$

The first term is a parabolic approximation to the track's circular trajectory in the xy plane, where κ is a function of the track's charge and transverse momentum and of the SLD

magnetic field. The second term represents the linear trajectory of the track in the rz plane, where λ is the track dip angle from the vertical. The σ parameters are the uncertainties in the track positions after extrapolation to $\vec{r}_0$ for the two projections. The function $f_i(\vec{r})$ is formed for each track i under consideration and used to construct the vertex probability function $V(\vec{r})$. Also included is $f_0(\vec{r})$, a $7 \times 7 \times 20$ μm ($x \times y \times z$) Gaussian ellipsoid centered at the IP position.

$$V(\vec{r}) = \sum_i f_i(\vec{r}) - \frac{\sum_i f_i^2(\vec{r})}{\sum_i f_i(\vec{r})} \tag{2}$$

Secondary vertices are found by searching for local maxima in $V(\vec{r})$ that are well-separated from the peak at the IP position. The tracks whose density functions contribute to such a local maximum are then identified as originating from a secondary vertex (SV).

A loose set of cuts is applied to tracks used for secondary vertex reconstruction. Tracks are required to have ≥ 2 VXD hits and $p_\perp > 250\,\mathrm{MeV}/c$. Tracks with 3D impact parameter > 3 mm or consistent with originating from a K_s^0 or Λ decay, or γ conversion are also removed. Each event is divided into two hemispheres using the thrust axis, and the vertexing procedure is performed in each using only the tracks in that hemisphere. The identified vertices are required to be within 2.3 cm of the center of the beam pipe to remove false vertices from interactions with the detector material. A cut on the secondary vertex invariant mass M of $|M - M_{K_S^0}| < 0.015$ GeV/c^2 removes any K_S^0 decays that survived the track cuts. The remaining vertices are then passed through a neural network [16] to improve the background rejection further. The input variables are the flight distance from the IP to the vertex (D), that distance normalized by its error (D/σ_D), and the angle ϕ_{PD} between the flight direction $\vec{D}$ and the total momentum vector of the vertex $\vec{P}$. These quantities are shown in Figure 3, along with the output value of the neural network (y_{vtx}). A good vertex in simulation is defined as one which contains only tracks from heavy hadron decays, with no tracks originating from the IP, strange particle decays, or other sources. Vertices with $y_{vtx} > 0.7$ are retained. At least one secondary vertex passing this cut is found in 72.7% of bottom, 28.2% of charm, and 0.41% of light quark event hemispheres in the Monte Carlo. Around 16% of the hemispheres in b events have more than one selected secondary vertex.

3.3 Track Attachment

Due to the cascade nature of b hadron decays, tracks from the heavy hadron may not all originate from the same space point. Therefore, a process of attaching tracks to the secondary vertex (SV) has been developed to recover this information using a second neural network. The first four inputs are defined at the point of closest approach of the track to the axis joining the secondary vertex to the IP. They are the transverse distance from the track to that axis (T), the distance from the IP along that axis to the POCA (L), that distance divided by the flight distance of the SV from the IP (L/D), and the angle of the track to the IP-SV axis (α). The last input is the 3D impact parameter of the track to the IP normalized by its error (b/σ_b). These quantities are shown schematically in Figure 4. The distributions are shown in Figure 5, along with the neural network output value (y_{trk}). The network is

Figure 3: Distributions of seed vertex selection variables: (a) distance from IP D, (b) normalized distance from IP D/σ_D, (c) angle between flight direction and vertex momentum ϕ_{PD}, (d) neural network output y_{vtx}. A good vertex contains only heavy hadron decay tracks. The arrow indicates the accepted region.

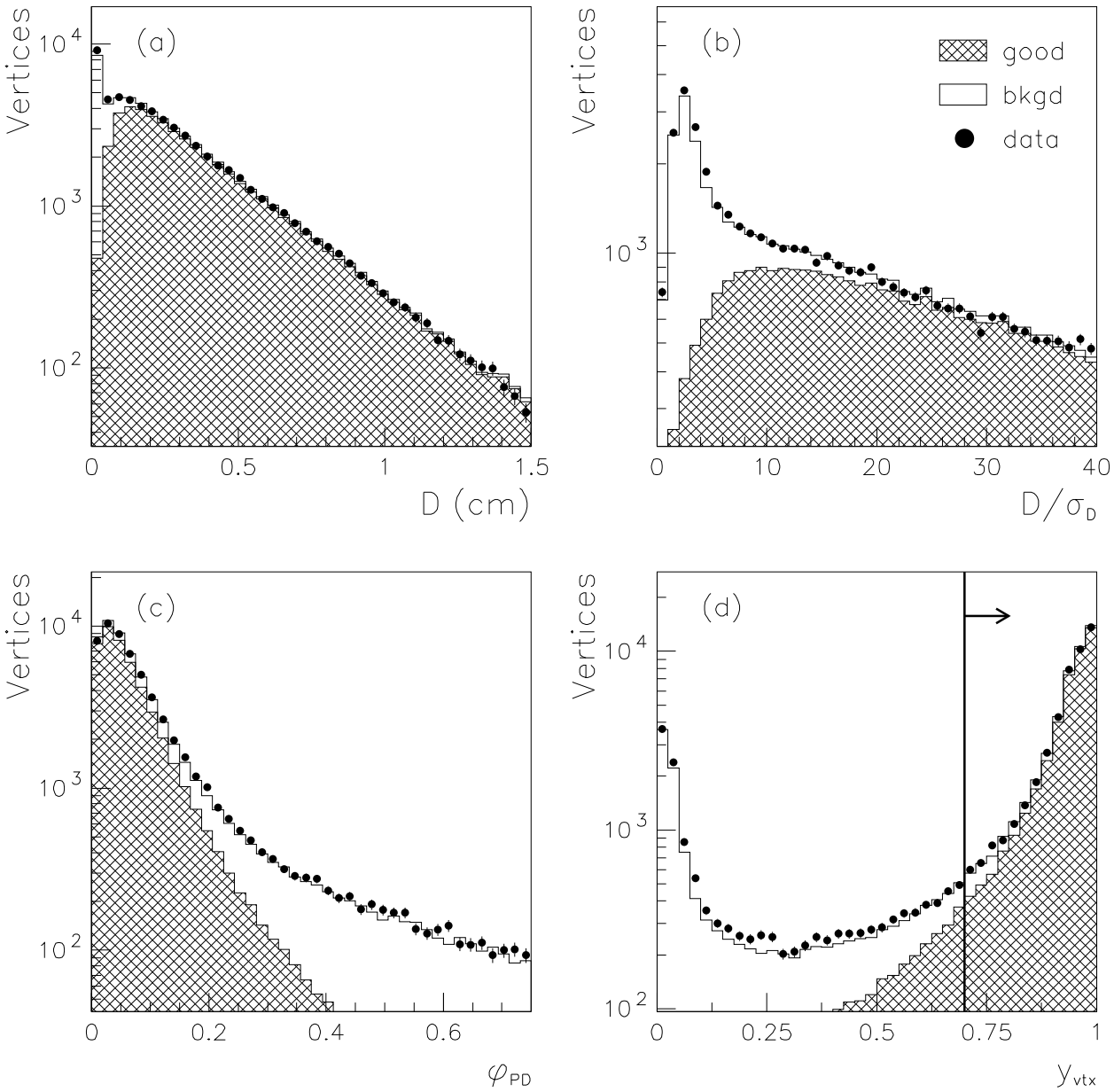

Figure 4: Schematic illustration of the quantities used in the track-attachment procedure described in the text (not to scale).

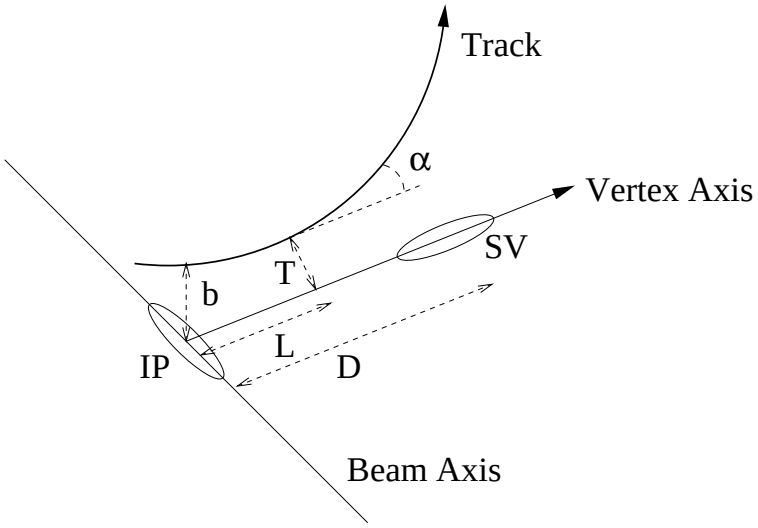

trained to accept only tracks which come from a b or c hadron decay, and to reject tracks from the IP or from strange particle decays or detector interaction products. If more than one secondary vertex was found in the hemisphere the attachment procedure is tried for each track-SV combination. Tracks with $y_{trk} > 0.6$ are added to the list of secondary vertex tracks. This value is chosen to minimize the number of fake tracks being attached to charm vertices, which than could mimic a b decay.

3.4 Flavor Discrimination

At this point, for each hemisphere there is a list of selected tracks. For hemispheres with no selected secondary vertices the list is empty, otherwise it includes the tracks in the secondary vertices and any cascade tracks which have been attached. From this list several signatures can be computed to discriminate between bottom/charm/light event hemispheres. These are the invariant mass of the selected tracks corrected for missing P_t (M_{hem}), the total momentum sum of the selected tracks (P_{hem}), the distance from the IP to the vertex obtained by fitting all of the selected tracks (D_{hem}), and the total number of selected tracks (N_{hem}).

The four signatures given above are used as inputs for a neural network trained to distinguish hemispheres in bottom/charm/light events. The four inputs and the neural network output y_{hem} are shown in Figure 6. The P_t corrected mass M_{hem} [2], is a particularly powerful discriminator to separate bottom and charm. For a detector with high precision vertexing capability, decay vertices from b and c hadrons can both be very distinctively separated from the IP at high efficiency. The large b hadron mass is then the key kinematic information to allow separation of $b\overline{b}$ and $c\overline{c}$ with high purity, which is crucial for these precision measure-

Figure 5: Distributions of the cascade track selection variables described in the text: (a) T, (b) L, (c) L/D, (d) α, (e) b/σ_b, (f) neural network output y_{trk}. A good track is one which originates from a heavy hadron decay. The arrow indicates the accepted region.

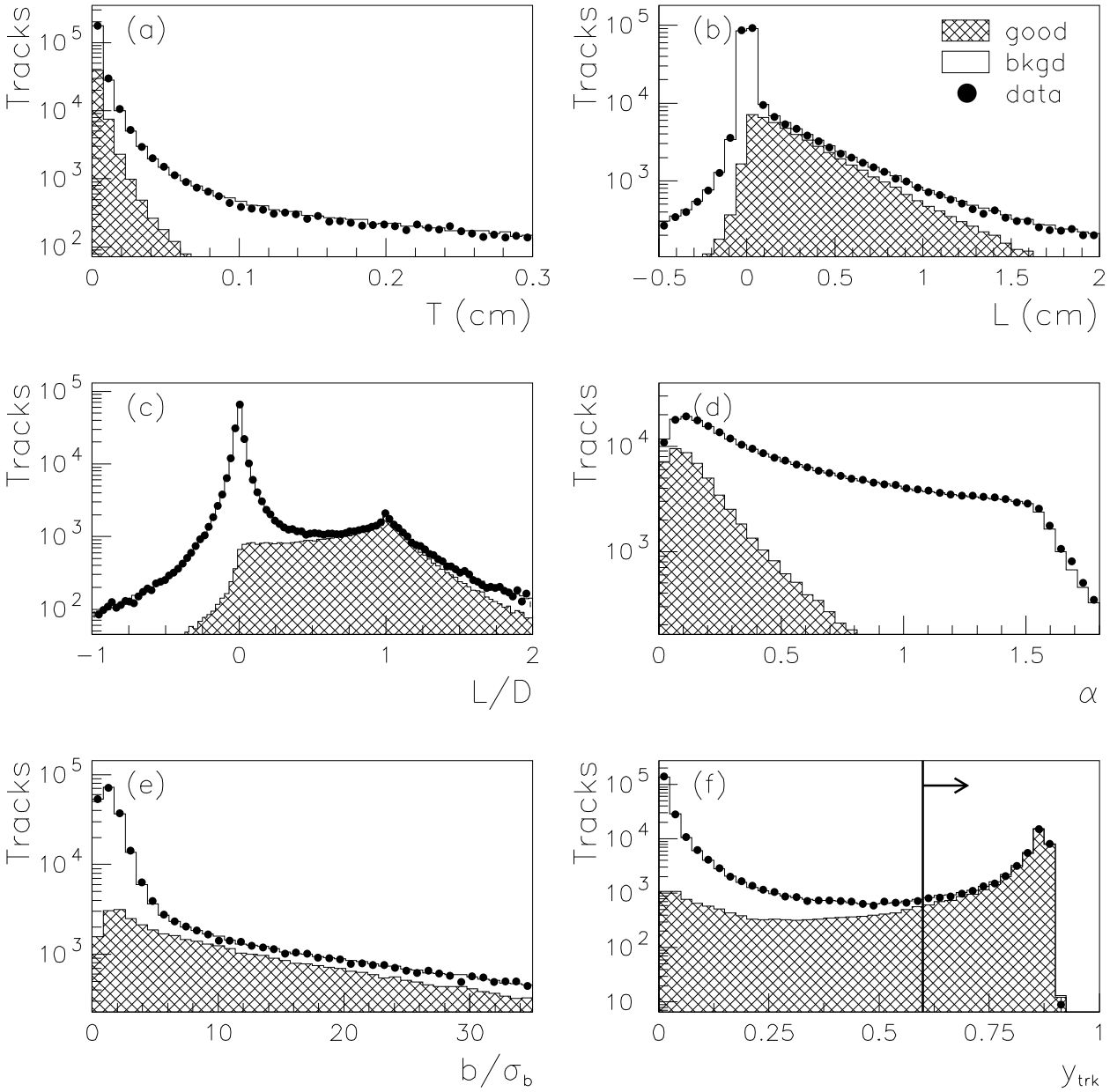

ments. The raw vertex mass from the selected charged tracks can already give high purity b tags once requiring mass above the charm threshold, but many b decays with missing neutrals have an apparent low vertex mass. With the secondary vertex and PV positions very precisely measured at SLD, the b hadron flight direction can be derived to compare with the vector sum of the selected secondary track momenta to estimate the missing P_t with respect to the b hadron flight direction. A corrected vertex mass is then calculated to compensate for the derived minimal missing mass, taking into account the vertex position errors:

$$M_{hem} = \sqrt{m_c^2 + P_t^2} + |P_t| \tag{3}$$

where m_c is the invariant mass of the tracks attached to the secondary vertex in the hemisphere.

Vertices in c quark jets, near the charm mass threshold typically have small missing P_t, while many b vertices near the charm mass threshold receive a large missing P_t correction to become well separated from $c\overline{c}$ events. The missing particles for the low mass b vertices generally lead to a lower apparent momentum calculated from the visible charged tracks so that the correlation between P_{hem} and M_{hem} presents another effective handle to further improve the flavor separation, as shown in (f) and (g) of Figure 6, comparing c and b jets.

The flavor selection neural network is trained to put charm event hemispheres near $y_{hem} = 0$, bottom event hemispheres near $y_{hem} = 1$, and light-flavor background near $y_{hem} = 0.5$. This allows a simple selection of charm (bottom) event hemispheres by specifying an upper (lower) limit for the output value y_{hem}. Figure 7 shows the ranges of purity vs. efficiency which can be obtained for charm and bottom event hemisphere tagging by adjusting this one cut. As can be seen in Figures 3 and 6, the inputs used for the neural networks at various stages of the y_{hem} tag construction are in reasonable agreement between data and MC. However, an exact agreement is not essential as the main tagging efficiencies will be measured directly from the data.

3.5 Vertexing Option Details

As a detailed internal reference, here are some of the specific options used for the vertexing. The vertexing and flavor tag analysis is through `B3MASS`, which in turn uses the `ZVTOP3` for the basic vertexing. The vertexingalgorithm is still original `ZVTOP` with pure geometrical vertexing (NOT the Ghost track version with more kinematic inputs). `B3MASS` modified a few default parameters of `ZVTOP3`, which are listed below for completeness:

```
zvkon3.tidy     1  Suppress K_s, Λ, γ-conversion vertices
zvkon3.zipe  20.0  IP z error (default=30)
zvkon3.rcut   0.8  vertex resolubility cut (default=0.6)
zvkon3.xcut   8.0  track vertex χ^2 contribution cut (default=10)
zvkon3.swim     1  Aaron's track swim error fix
```

Figure 6: Distributions of flavor discrimination variables: (a) M_{hem}, (b) P_{hem}, (c) D_{hem}, (d) N_{hem}, (e) neural network output y_{hem}, (f) P_{hem} vs. M_{hem} correlation for c jets (g) same for b jets.

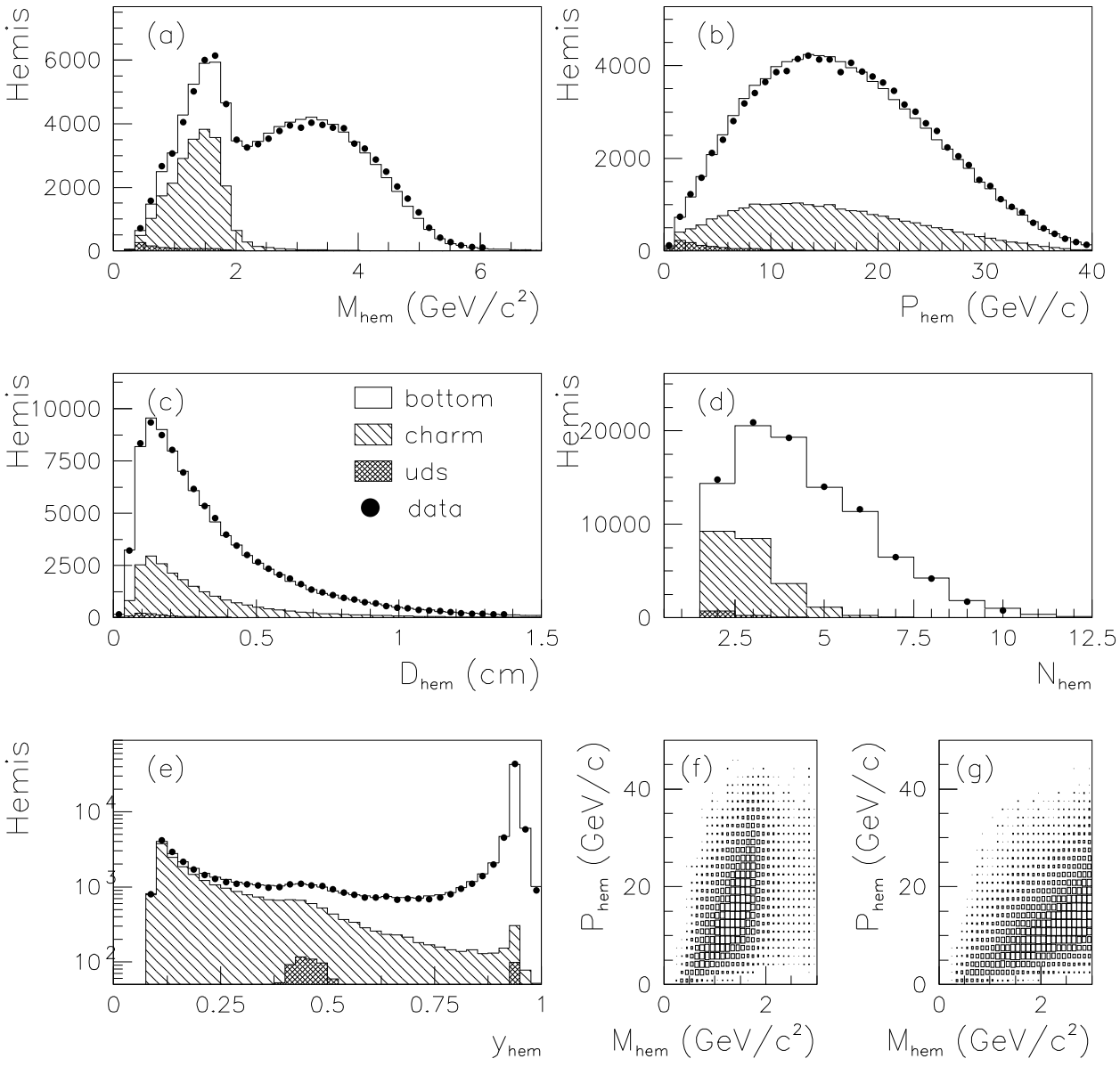

Figure 7: Purity vs. efficiency for hemispheres in (a) charm and (b) bottom events, as the selection neural network cut is varied.

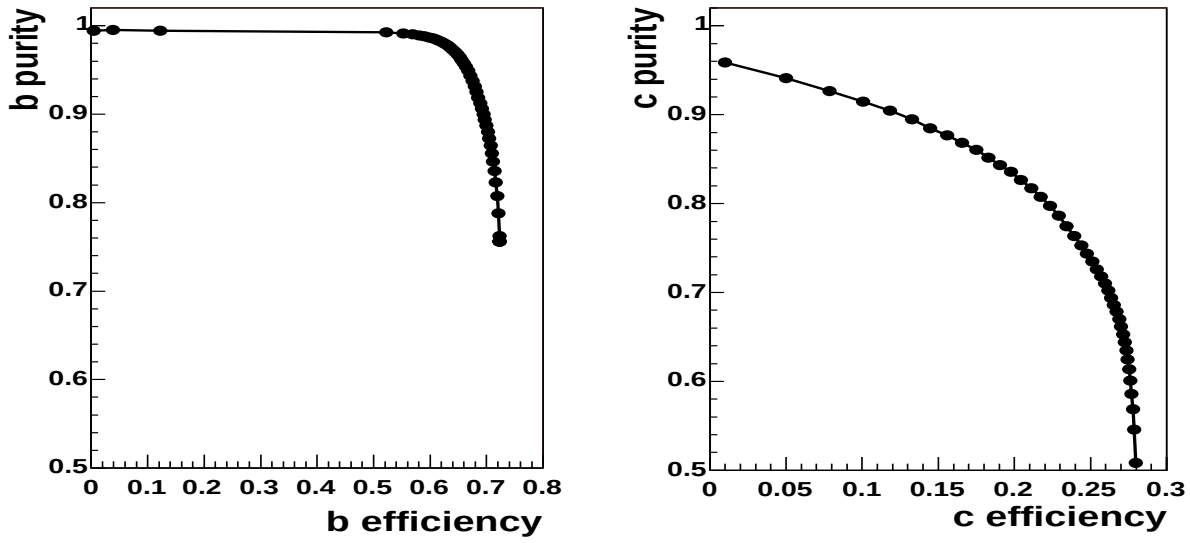

4 Measurement Method and Results

Each event is divided into two hemispheres by the plane perpendicular to the thrust axis. Both measurements apply flavor tags on each hemisphere separately to derive R_b and R_c, and measure the major tagging efficiencies from data simultaneously.

4.1 R_b measurement

For the R_b measurement, we define a single b-tag with y_{hem} >0.75 and apply the classical double tag method as in our previous measurement [2]. By counting the fraction of tagged hemispheres, F_s, and the fraction of events with both hemispheres tagged, F_d, we can measure R_b by iteratively solving the following equations:

$$\begin{aligned} F_s &= \epsilon_b R_b + \epsilon_c R_c + \epsilon_{uds}(1 - R_b - R_c), \\ F_d &= C_b \epsilon_b^2 R_b + C_c \epsilon_c^2 R_c + \epsilon_{uds}^2 (1 - R_b - R_c). \end{aligned} \quad (4)$$

where $\epsilon_{uds}, \epsilon_c$ and ϵ_b are the hemisphere tagging efficiencies for uds, c and b hemispheres, respectively, and $C_q = \frac{\epsilon_q^{double}}{\epsilon_q^2}$, are the hemisphere tag correlations for b and c events. We ignore the correlation for uds events since we expect 0.23 double tagged events. A Standard Model value of R_c=0.1723 is assumed. The dependence on MC simulation is greatly reduced by measuring ϵ_b from data, while only the small ϵ_c,ϵ_{uds} and correlations are estimated from MC. The measurement results and estimated MC parameters are tabulated in Table 2 for

the 96 and 97-98 data samples. The errors are statistical only for both measured and MC parameters. The R_b result has been corrected by -0.00149 for hadronic event selection bias and by $+0.00030$ for $Z\gamma$ interference effect.

	96			97-98		
R_b	0.21438	$\pm$	0.00289	0.21630	$\pm$	0.00104
ϵ_b(data)(%)	56.63	$\pm$	0.67	62.01	$\pm$	0.24
ϵ_b(MC)(%)	56.91	$\pm$	0.08	61.78	$\pm$	0.03
Π_b (%)	97.8	$\pm$	0.4	97.9	$\pm$	0.1
ϵ_c(MC)(%)	1.24	$\pm$	0.02	1.19	$\pm$	0.01
ϵ_{uds}(MC)(%)	0.113	$\pm$	0.006	0.134	$\pm$	0.003
$C_b - 1$(MC)	0.0067	$\pm$	0.0015	-0.00012	$\pm$	0.00049
$C_c - 1$(MC)	0.16	$\pm$	0.26	0.30	$\pm$	0.12
N events	29996			191770		
N single tag	3315			20738		
N double tag	2091			16048		

Table 2: R_b result and tagging performance parameters. Π_b is the hemisphere b-tag purity. All errors are statistical only.

4.2 R_c measurement

Unlike the case of the R_b measurement where the single $y_{hem} > 0.75$ tag has already collected b hemispheres with both high efficiency and high purity, the charm events are more spread out in the y_{hem} distribution. Since the number of double tagged events is very sensitive to the tag efficiency, the lower efficiency for charm tagging makes the use of different tags with quite different purities more profitable. We therefore use a multi-tag approach for the R_c measurement.

We divide hemispheres with a secondary vertex into four tag categories, depending on the output value of the neural network, y_{hem}. A b tag (tag 4) with $y_{hem} > 0.75$, a charm tag (tag 1) with $y_{hem} < 0.3$, a low-purity b-tag (tag 3) with $0.5 < y_{hem} < 0.75$ and a low-purity charm tag (tag 2) with $0.3 < y_{hem} < 0.5$. Hemispheres without a secondary vertex are classified in the tag 0 category. In total we have 15 different event categories $N_{ij}, i \leq j \leq 4$ for the different tag combinations with a predicted fraction of the number of events G_{ij} :

$$G_{ij} = \kappa[\epsilon_b^i \epsilon_b^j C_b^{ij} R_b + \epsilon_c^i \epsilon_c^j C_c^{ij} R_c + \epsilon_{uds}^i \epsilon_{uds}^j C_{uds}^{ij} (1 - R_b - R_c)] \tag{5}$$

with $\kappa = 1$ for $i = j$ and 2 for $i \neq j$. ϵ_q^i is the efficiency for quark q to give a tag i. C^{ij} is the tag correlation between tag i and tag j similarly defined as in the R_b case. Since N_{00} is determined by the total number of events and the other event counts, we have 14 independent equations for the event fractions $F_{ij} = N_{ij}/N_{\text{total}}$.

A small number of uds events produce a secondary vertex. This has two reasons. The first is gluon splitting to $b\overline{b}$ and $c\overline{c}$. The result is a real heavy quark of which the decay

is well modeled in our simulation. These events mainly populate the high purity b and c tag categories and the errors on the measured rates dominate the systematic uncertainty assigned to this effect. The other source is incorrect reconstruction in our detector. These events typically cluster around $y_{hem} = 0.5$. This is less well modeled, and in the next section we estimate the error on the rate predicted by our simulation to be 10%. The N_{02} and N_{03} categories contain most of these events. To avoid a bias from these low purity bins, we de-weight them by taking as the error on the event fraction, $\sigma_{F_{ij}}$, the binomial error on the bin contents and the systematic effect from varying the non-gluon splitting uds efficiency by 10%, added in quadrature.

We minimize

$$\chi^2 = \Sigma_{i,j,i\leq j}(F_{ij} - G_{ij})^2/(\sigma_{F_{ij}})^2 \tag{6}$$

as a function of the following 9 parameters: R_b, R_c, ϵ_b^j $(j = 1, 4)$ and ϵ_c^j $(j = 1, 3)$. The c-quark efficiency for the b-tag, ϵ_c^4, all light quark efficiencies, ϵ_{uds}^j $(j = 1, 4)$ and the hemisphere correlations C_q^{ij} are taken from Monte Carlo. Only a few of the correlations are different from 1 in a statistically significant way. The others are set to 1.

The R_c fit results are summarized in Table 3. The R_c values have been corrected by -0.0003 for $Z\gamma$ interference, the event selection bias is zero in simulation. The R_c values are given at a central R_b value of 0.2157. The measured value of R_b agrees with the determination from the R_b measurement. There is a good agreement between the efficiencies in Monte Carlo and Data in the high purity tags 1 and 4. The efficiency for the lower purity tags 2 and 3 for charm is higher in Monte Carlo than in the 97-98 data sample. The Monte Carlo efficiency is quite sensitive to physics parameters like the charmed hadron production fractions, their decay multiplicities and their lifetimes. The measured value of the efficiency can be reproduced in the Monte Carlo, by varying some of these parameters within their allowed range as is done in the study of systematic uncertainties. Since we extract the efficiencies from the data, the measured value of R_c is insensitive to these variations.

5 Systematic Errors and Cross-checks

The systematic uncertainties on R_b and R_c, given in detail in Table 13, result from a combination of detector related effects and physics uncertainties in the simulation which affect our estimates of ϵ_c, ϵ_{uds} and C_q in the case of R_b and ϵ_4^c, ϵ_i^{uds} and all correlations for R_c. These systematic errors listed in Table 13 are for the combined results for 96 and 97-98 data which are analyzed separately initially.

The double tag algorithm places high premium on the tagging efficiency as the number events required for a particular statistical precision is proportional to $1/\epsilon^2$. At the same time, the high tagging efficiency is also beneficial to the tagging purity for reducing systematics. In the simple double tag case for the R_b measurment, the dependence of the R_b systematic on the various parameters can be expressed as:

$$\delta R_b \sim \frac{-2R_{uds}\epsilon_{uds}}{\epsilon_b} \cdot \frac{\delta\epsilon_{uds}}{\epsilon_{uds}}$$

	96		97-98	
	data	MC	data	MC
R_c	0.1679 ± 0.0091		0.1753 ± 0.0033	
ϵ_b^1 (%)	2.22 ± 0.18	2.01	2.52 ± 0.07	2.36
ϵ_c^1 (%)	16.09 ± 0.90	15.74	17.95 ± 0.36	18.43
ϵ_{uds}^1 (%)		0.088		0.063
ϵ_b^2 (%)	2.83 ± 0.20	2.56	2.97 ± 0.07	3.00
ϵ_c^2 (%)	4.93 ± 0.36	4.94	5.02 ± 0.13	5.74
ϵ_{uds}^2 (%)		0.117		0.124
ϵ_b^3 (%)	4.68 ± 0.24	4.40	5.10 ± 0.09	4.98
ϵ_c^3 (%)	2.46 ± 0.27	2.62	2.23 ± 0.10	2.90
ϵ_{uds}^3 (%)		0.150		0.140
ϵ_b^4 (%)	56.8 ± 0.64	56.9	62.18 ± 0.23	61.78
ϵ_c^4 (%)		1.24		1.19
ϵ_{uds}^4 (%)		0.113		0.134
$C_c^{11} - 1$		-0.0068		0.012
$C_b^{14} - 1$		0.0032		0.0011
$C_b^{34} - 1$		0.0064		-0.0015
$C_b^{44} - 1$		0.0067		-0.00012
other $C_q^{ij} - 1$		0		0
$\chi^2/d.o.f.$	6.66/5		7.05/5	

Table 3: R_c results and tagging performance parameters. The errors on the MC efficiencies are small compared to systematic uncertainties and therefore omitted

$$
\begin{aligned}
\delta R_b &\sim \frac{-2R_c\epsilon_c}{\epsilon_b} \cdot \frac{\delta\epsilon_c}{\epsilon_c} \\
\delta R_b &\sim \frac{-2\epsilon_c}{\epsilon_b} \cdot \delta R_c \\
\delta R_b &\sim R_b \cdot \delta C_b \\
\delta R_b &\sim \frac{R_c\epsilon_c^2}{R_b\epsilon_b^2} \cdot \delta C_c
\end{aligned}
$$

It can be seen that the controlling factors for the light flavor background are $\frac{\epsilon_{uds}}{\epsilon_b}$ and $\frac{\epsilon_c}{\epsilon_b}$. In the case of correlations, the C_c dependence is negligible at the normal operating point, but it becomes relevant when looking at R_b variation as a function of the y_{hem} cut for the very loose cut region. For the tagging correlations, operating at a large tagging efficiency regime is also very effective in reducing the correlation and its uncertainty.

5.1 Hemisphere correlation component analysis

With the statistical precision down to $< 0.5\%$ level for R_b and $< 2\%$ for R_c, the systematic uncertainties of the small subtle effects of hemisphere tag correlation become important.

As the correlations have variety of origins and the evaluation of their uncertainties will be spread over many subsections to follow, we will first discuss the correlation sources to establish an understanding of the magnitude of their effects. Primarily as a cross check to constrain possible missing systematic sources for the hemisphere correlations, we decompose the efficiency correlation of the b and c tags into a set of independent components which represent the major known sources of correlation between the two hemispheres in the $b\overline{b}$ and $c\overline{c}$ MC events.

To focus on understanding the physics sources, we use the large uniform 97-98 MC sample without tracking efficiency and resolution corrections. The tracking corrections tend to introduce random fluctuations which can confuse the picture and their effect will be evaluated separately in the detector systematic section. For the R_c measurement, there are many correlations between the different tags. We only examine a representative c-tag of $y_{hem} < 0.4$, for similar set of effects as for the b-tag. For this study we need to identify the relevant kinematic and geometric variables to see how the tagging efficiencies depend on them and how the two hemispheres correlate on these variables which then translate to tagging correlations.

The primary vertex (PV) shared between the two hemispheres is an obvious source of correlation. Misreconstructed PV can result in negative correlations between the hemispheres if PV displacement is along the thrust axis. Transverse PV displacement would tend to positively correlate the two hemipheres. The small and stable SLD IP in the xy view is an average beam position over many events which greatly reduces the chance of large PV displacement in the xy. The PV z reconstructed event by event, can have more ways to allow two hemispheres influencing each other through PV bias. The total PV effect is studied by simply comparing using the reconstructed PV and using the MC truth PV.

Another major source is geometric correlations. The two hemispheres are always exactly back to back, and in particular one hemisphere at polar angle $\cos\theta$ makes the other hemisphere necessarily at $-\cos\theta$ has major potential for correlation. Due the cylindrical geometry of the detector, larger $|\cos\theta|$ typically mean more multiple scattering, worse tracking efficiency and worse resolution for radial alignment effect etc. We calculate the tagging efficiencies for each hemisphere axis $\cos\theta$ bin to construct a function of $\epsilon(\cos\theta)$. The $\cos\theta$ correlation component can then be estimated from

$$C = \sum_i \epsilon(\cos\theta_i) \cdot \epsilon(-\cos\theta_i)\, f(\cos\theta_i)/\overline{\epsilon}^2$$

where i is the index of the $\cos\theta$ bin, f is the fraction of all events in bin i and $\overline{\epsilon}$ is the average tagging efficiency of all hemispheres.

Although the cylindrical geometry of the detector ensures uniformity at first order in azimuth, local performance degradation of detector elements can introduce an effect still. Similar to the θ component analysis, the ϕ component is estimated from

$$C = \sum_i \epsilon_{forward}(\phi_i) \cdot \epsilon_{backward}(\phi_i + \pi)\, f(\phi_i)/\overline{\epsilon}^2$$

where the efficiency parameterization is done for forward ($+z$) and backward ($-z$) hemispheres separately.

As a symmetric concern compared to the spatial nonuniformity, tagging correlation due to variation of detector performance in time also needs to be addressed. This is in fact the primary reason that the 978 data and 96 data are analyzed separately. The 96 data not only had electronics problems which caused some VXD3 ladders to be missing at certain periods, there is also an overall worse VXD3 hit inefficiency due to the more pronounced radiation damage effect while we ran at higher temperature. The radiation damage effects are largely removed for the much larger 97-98 data sample when the VXD3 ran at ∼10 degrees colder, in addition to the electronics repairs. The Monte Carlo simulation has been carefully following these time dependent effects in detail. The MC signal tagging efficiencies as a function of the run numbers are shown in Fig. 8. The time dependence component is estimated from

$$C = \sum_i \epsilon^2(R_i)\, f(R_i)/\overline{\epsilon}^2$$

where R_i is a group of runs adjacent in time, $f(R_i)$ is the fraction of all events in this group of runs.

The b/c-tag efficiencies have a significant dependence on the corresponding heavy hadron momentum (P_H) and its angle to the hemisphere axis (ξ). There are various causes, in particular gluon radiations, which can result in correlations of heavy hadron momenta and angular distributions. We parameterize the hemisphere tagging efficiency in a 2D grid of $\epsilon(P_H, \xi)$ then integrate the correlation for hemispheres 1 and 2 of each event i:

$$C = \sum_i \epsilon(P^i_{H1}, \xi^i_1) \cdot \epsilon(P^i_{H2}, \xi^i_2)/\overline{\epsilon}^2$$

This component is only evaluated for the normal cases where two heavy hadrons are in opposite hemispheres. The joint effect of the heavy hadron momentum and thrust angle is ∼20% larger than the effect from momentum alone.

For the extreme case of hard gluon radiation, with two heavy quarks recoiling into the same hemisphere opposite the hard gluon, we simply calculate the effect from including and excluding these events in the overall sample. The magnitude of the various components and their sum compared with the overall correlations calculated from the MC hemisphere and double tag rates are shown in Table 5.1. An important observation is that the magnitude of all components are small, which is especially true for the b-tag. The change in the value of the correlation C translates to the fractional error of R_b and R_c. So the effect at typically 0.1% (1%) or less for the b-tag can be compared with the R_b (R_c) statistical error of ∼0.5% (2%). This illustrates the importance of the large tagging efficiency in driving a much smaller correlation and reduce sensitivity to correaltion uncertainties, which is even apparent when comparing the b-tag with the c-tag. A more naive way to understand this is that in the limit of 100% tagging efficiency, the correlation becomes irrelavant.

The 96 samples are not large enough to draw detailed conclusions goven the large MC statistical error. However, the effects in time and geometrical correlations due to the varied detector performance in 96 are clearly quite significant and their component magnitude describe well the difference of the overall correlation between 96 and 97-8. For the more precise tests of the 97-98 samples, there is a noticeable discrepancy between the b-tag component

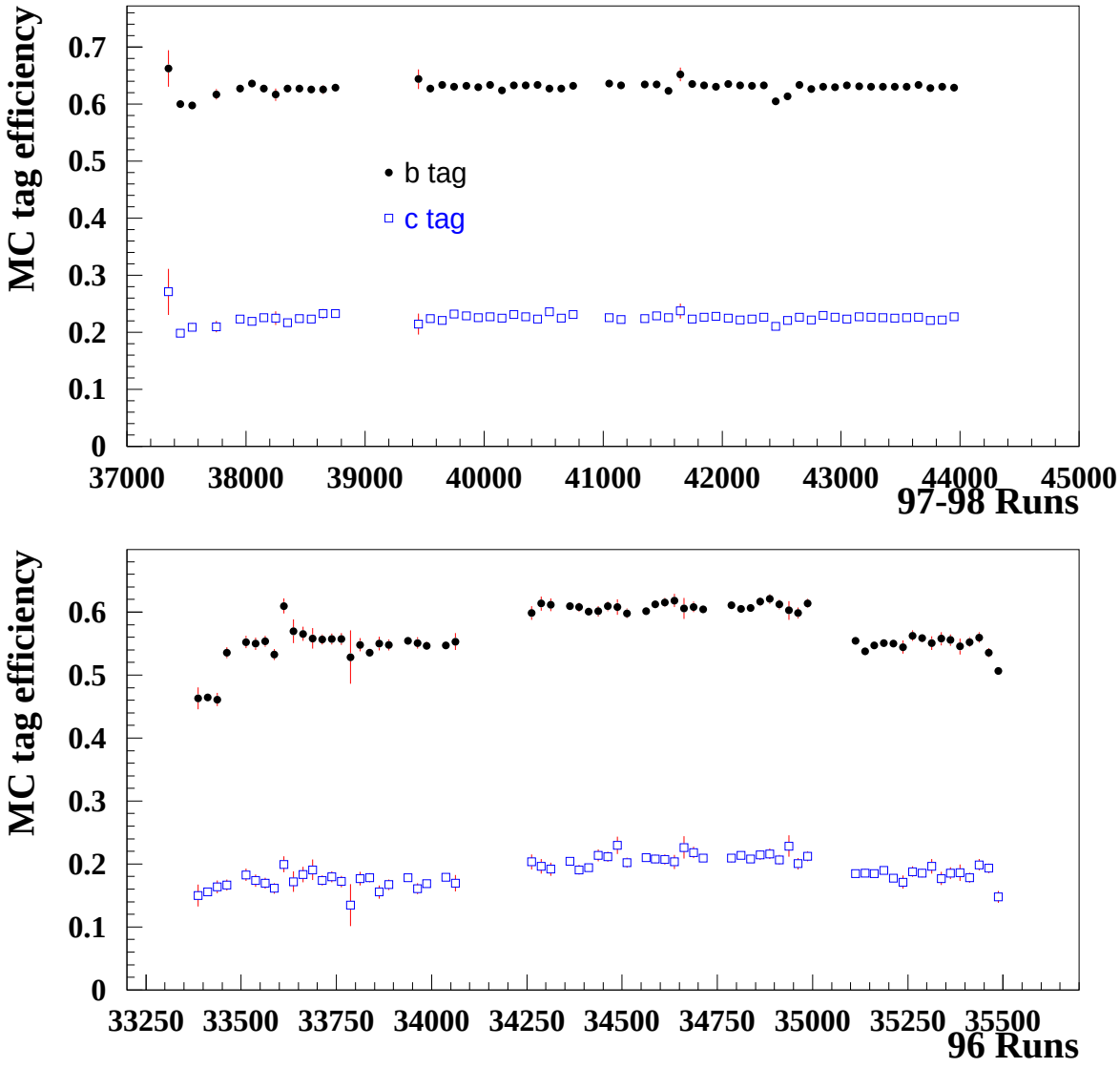

Figure 8: MC simulated tagging efficiencies as function of time.

Component	$(C_{b-tag}-1)\times 10^5$		$(C_{c-tag}-1)\times 10^5$	
	97-98	96	97-98	96
Primary vertex	+46	+13	−480	−640
B/D momentum and thrust angle	+107	+95	+820	+760
Hard gluon radiation	−37	−23	+510	+410
Geometrical correlation θ	+49	+60	+120	−120
Geometrical correlation ϕ	−4	+212	−10	+170
Time dependence	11	+434	+40	+870
Component sum	+170	+670	+1000	+1450
MC overall correlation	+42	+891	+420	+1510
MC statistical error	±47	±113	±390	±1210
Discrepancy	+128	−121	+580	−60

Table 4: Hemisphere correlation component check results for b-tag and c-tag.

sum and the MC overall correlation. Although at least part of the discrepancy could be statistical for this approximate cross check, we take half of discrepancies from the 97-98 analysis for both the b-tag and c-tag as an additional systemtic error for possible missing sources.

To comprehend these results and to get a better feel of the behaviors of the tags, we include some related plots in this note for completeness. The b-tag efficiency as a function of $\cos\theta$ and other production and decay variables, is shown in Fig. 9. The tagging efficiency is almost a constant up to $\cos\theta$ ∼0.6 and drops by 10% up to 0.7. This relatively weak dependence is probably largely owing to the low multiple scattering and constant spatial resolution vs θ for VXD3. For the charm tag $y_{hem} < 0.4$, the tag performance is looked at together with a few other MC variables (not all related to correlations) as shown in Fig. 10. The $\cos\theta$ variation is again small. There are clearly some footprint of the b-c separation neuralnet trying to distinguish the charm from b, such that the more obvious high multiplity decays, long distance decays (more like b's) are not necessarily favored by the c-tag. Instead, it likes intermediate decay multiplicities of 3-4 at short decay length.

The B/D momentum and thrust angle correlation is probably the most complex and hardest to visualize. Variety of ways of looking at the tag dependences, population densities and correlations are shown in Fig. 11, Fig. 12 and Fig. 13 for b-tag and corresponding set of plots in Fig. 14, Fig. 15 and Fig. 16 for c-tag.

The tagging efficiencies very quickly ramping up to an efficiency plateau at P=20 GeV for the heavy hadron momentum is a quite impressive sight. This helps to reduce sensitivity to momentum correlation. The old VXD2 mass tag or typical tags at LEP mostly have a steeper ramping across most of the spectrum. The sensitivity of tagging efficiency to the angle from the thrust axis, is probably at least in part due to the fact that ZVTOP is preferentially searching for vertices along a tube around the hemisphere axis. Heavy hadrons kicked sideways by gluon emission and travelling a long distance may become particularly vulnerable. However, the effect is not as dramatic as seen in the overall efficiency vs. thrust

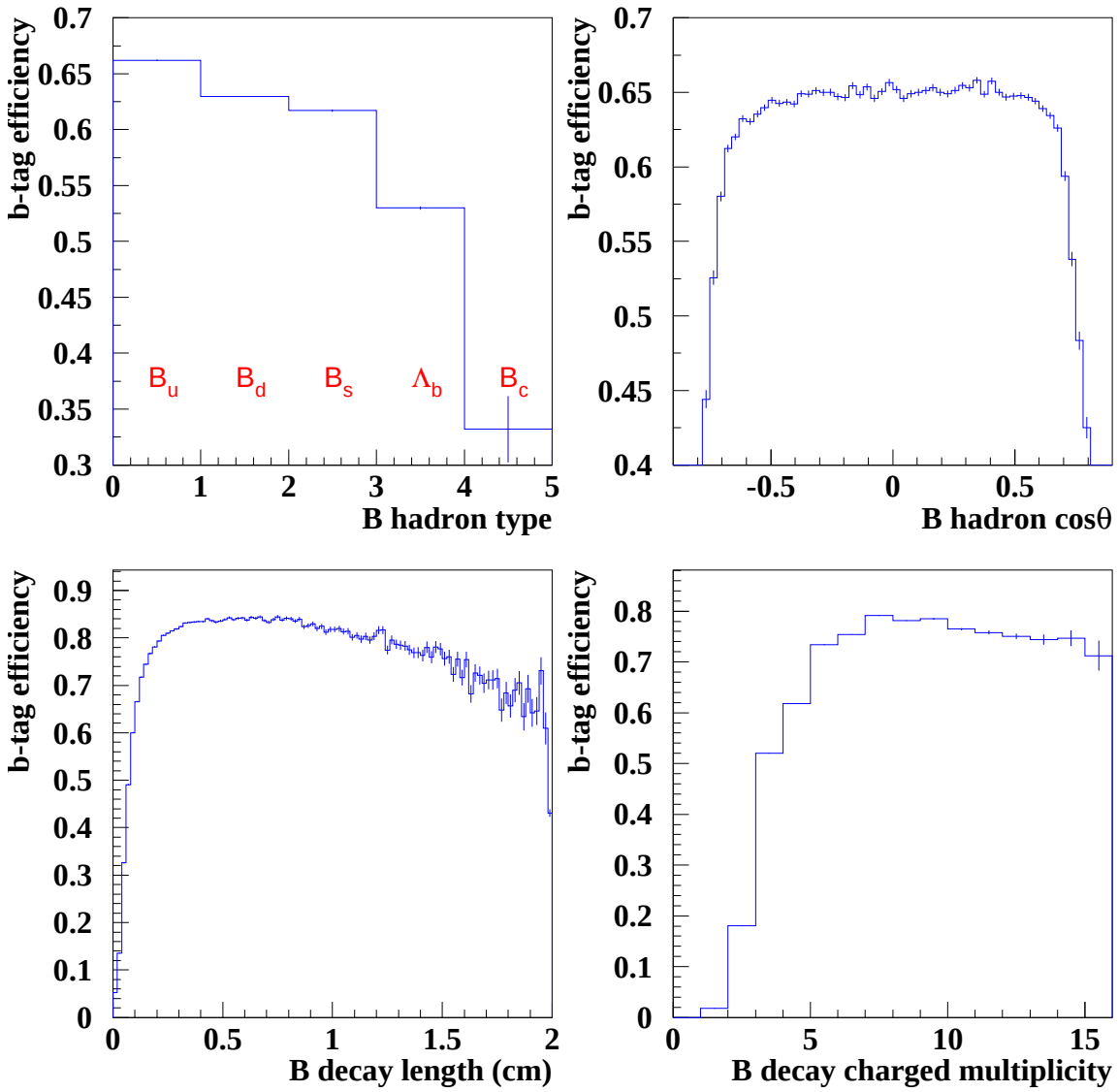

Figure 9: MC b-tag efficiency as a function of various b-hadron production and decay variables.

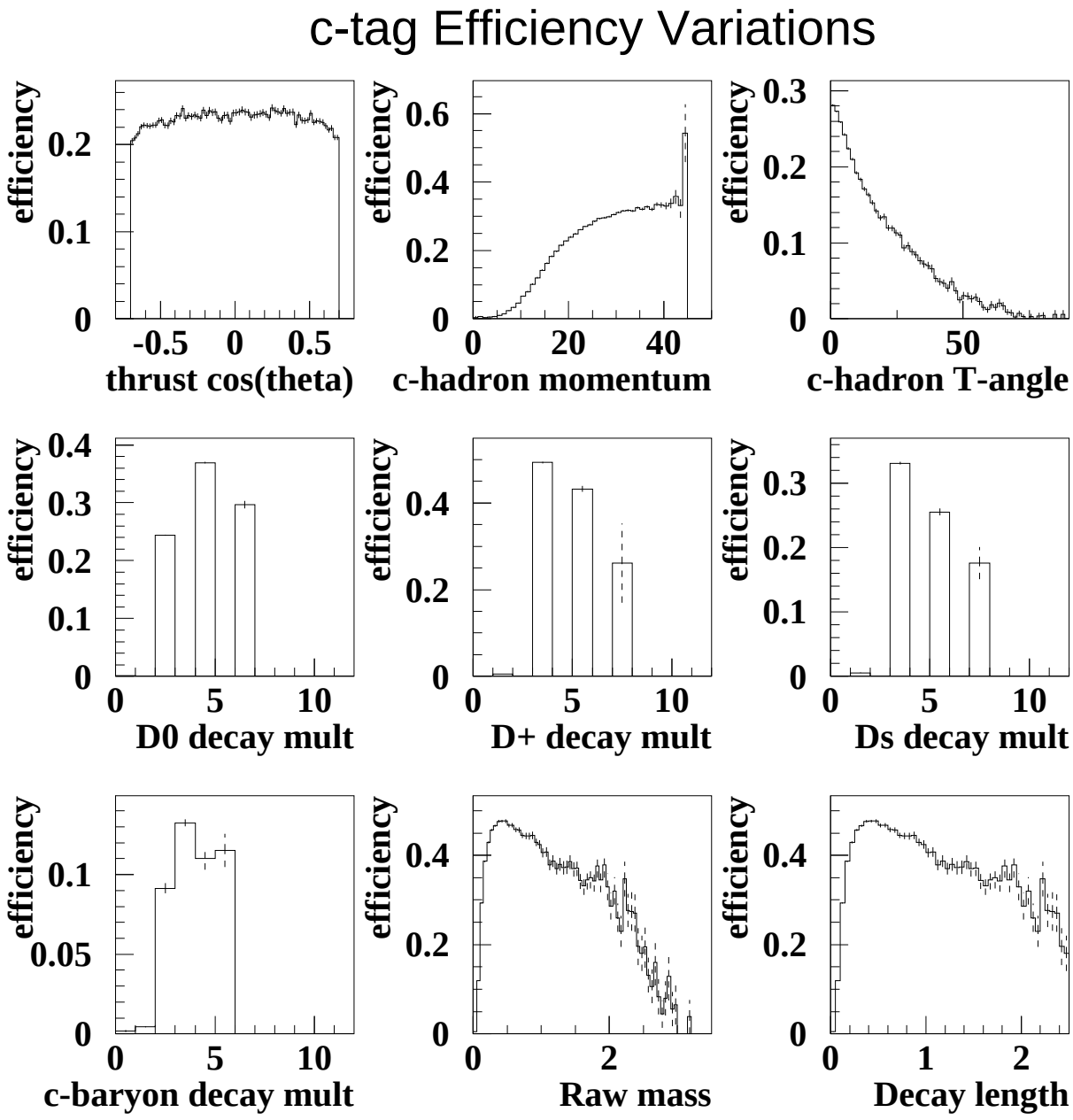

Figure 10: MC c-tag efficiency variations as functions of various production and decay parameters.

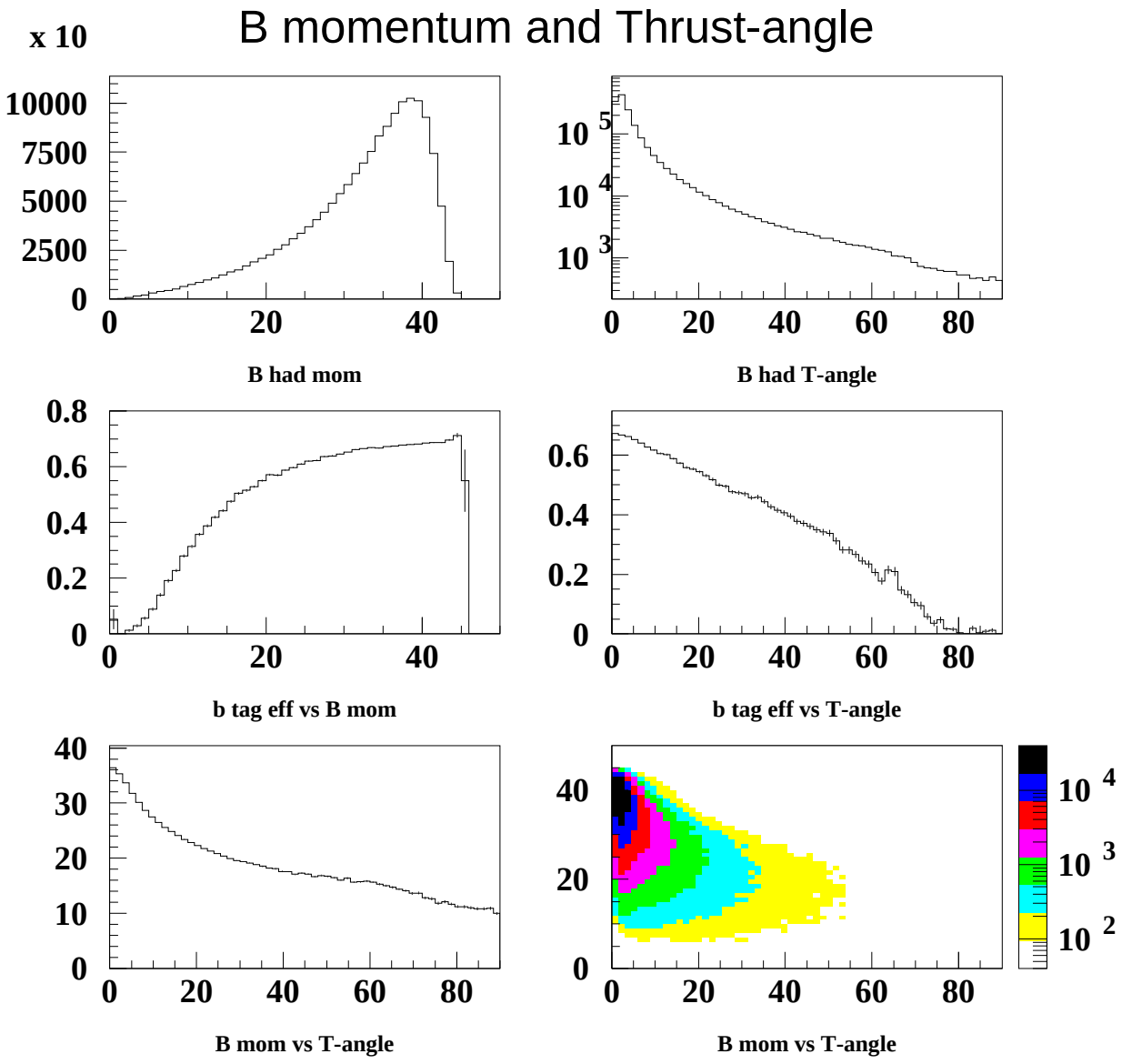

Figure 11: Summay of MC b-tag efficiency variations as functions of B momentum and thrust angle.

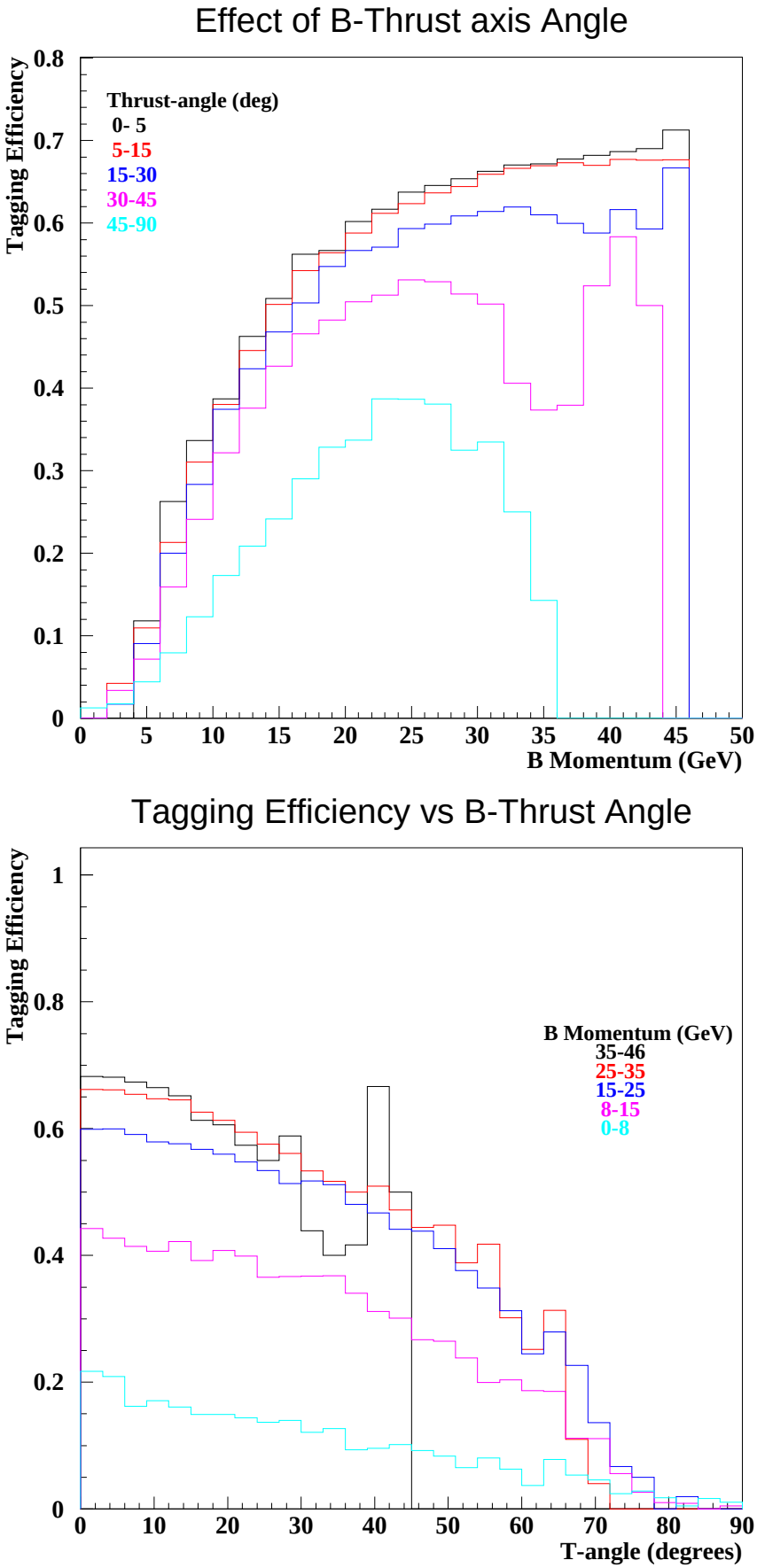

Figure 12: MC b-tag efficiency variations as functions of B momentum and thrust angle in fixed range slices.

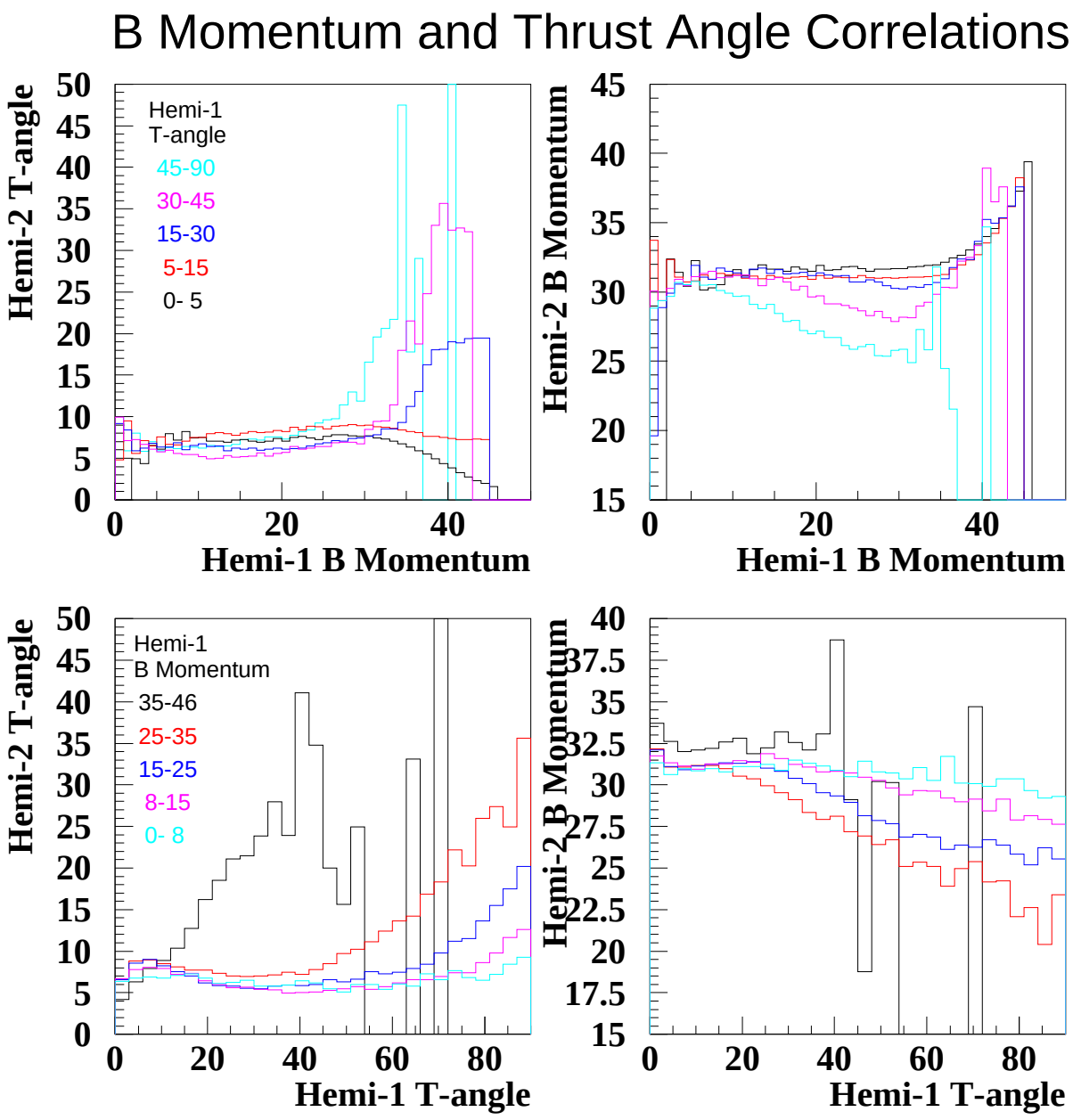

Figure 13: MC B production momentum and thrust angle correlation.

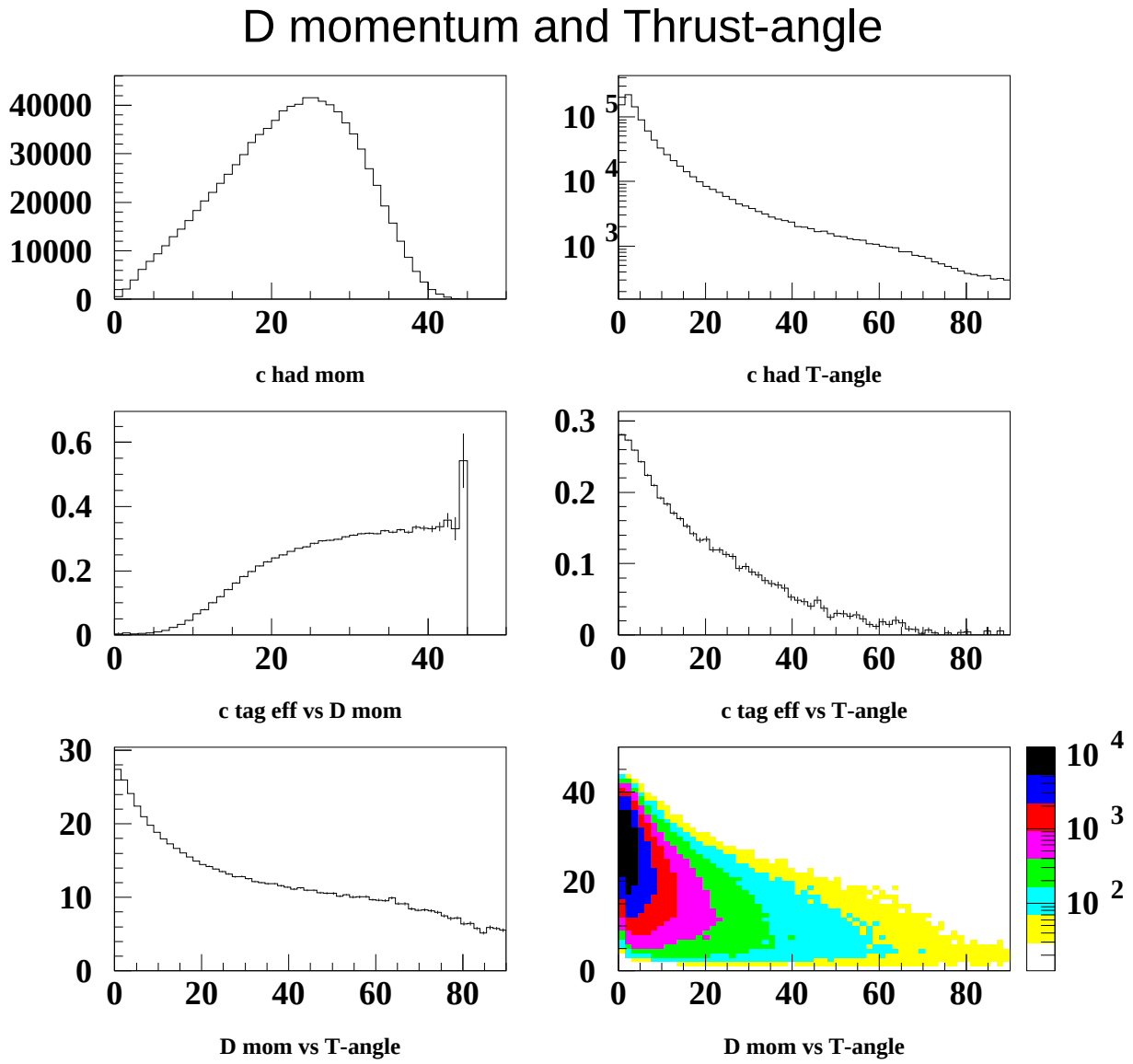

Figure 14: Summay of MC c-tag efficiency variations as functions of D momentum and thrust angle.

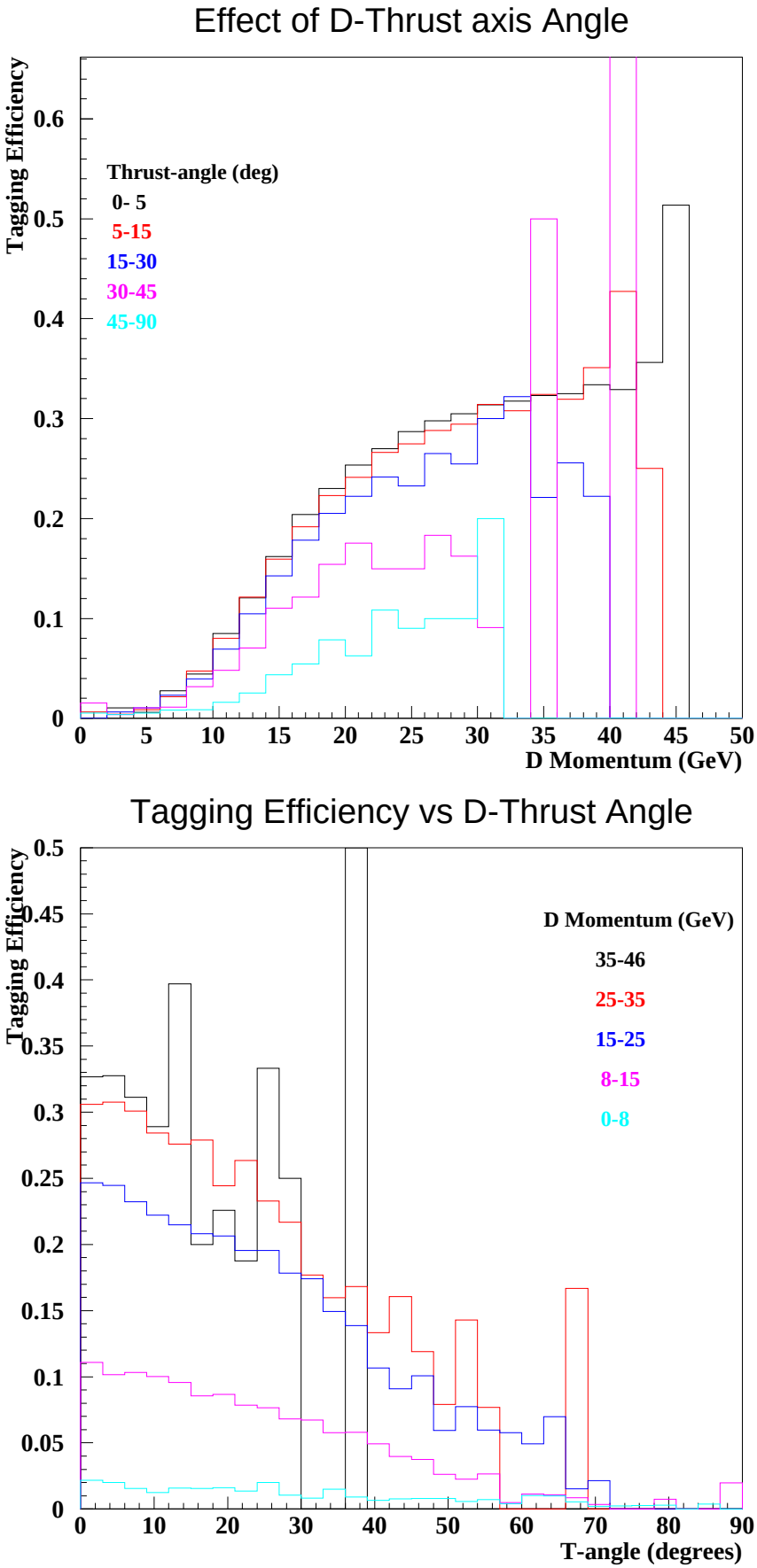

Figure 15: MC c-tag efficiency variations as functions of D momentum and thrust angle in fixed range slices.

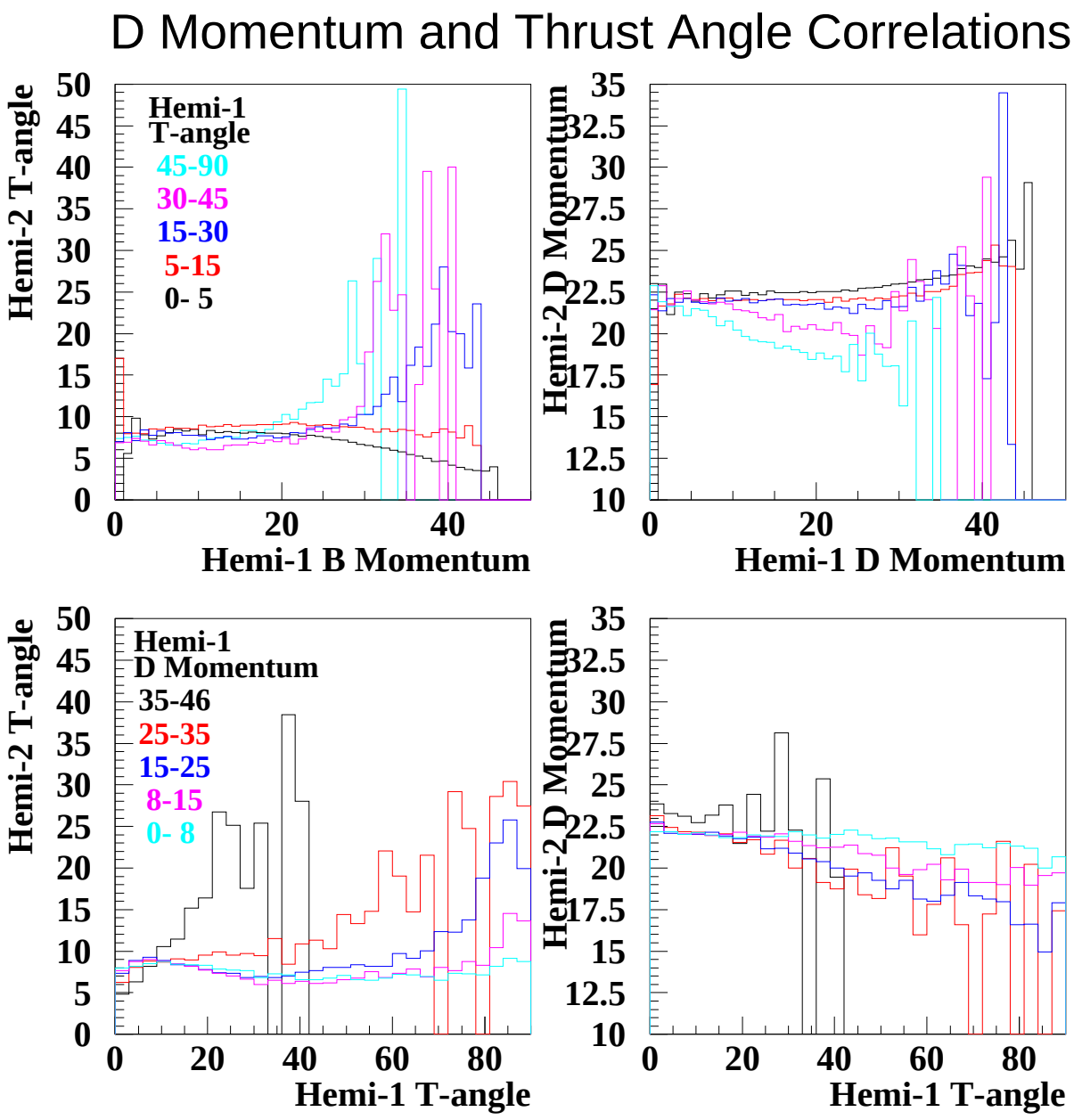

Figure 16: MC $c\bar{c}$ D production momentum and thrust angle correlation.

	$g \to c\bar{c}$ (%)	$g \to b\bar{b}$ (%)
JETSET	1.357	0.142
LEPEWWG standard	2.96±0.38	0.254±0.051

Table 5: The world average measurements of $g \to Q\overline{Q}$ compared to JETSET generator.

angle plot would suggest. The heavy hadrons kicked to large angles also typically have lower momenta. So it is fairer to look at the thrust angle dependence for fixed heavy hadron momentum slices, although the effect is still very significant. It may be tempting to consider running the vertexing analysis on jets instead of hemispheres, but that will bring the complication of how to implement a double tag algorithm when there are more than 2 jets in the event. We decided not to embark on a major change of analysis paradigm at this late stage.

5.2 Physics systematics

The physics systematic errors are mostly assigned by reweighting the nominal simulated distributions to an alternative set of distributions which correspond to the world average measurements and uncertainties of the underlying MC physics parameters [17].

5.2.1 $g \to Q\overline{Q}$ effect

The $g \to b\bar{b}$ and $g \to c\bar{c}$ production rates are varied according to the experimental averages [17]. These measurement rates are significantly higher than the default JETSET MC as shown in Table 5, so that corrections to central values and variations are evaluated for all efficiencies and correlations. The main sensitivity to the gluon splitting uncertainties is through the uds tagging efficiencies. Its effect on charm background under the b-tag is also noticeable. In the case of R_b measurement, we can see in detail how $g \to Q\overline{Q}$ affects the various parameters and the corresponding effect on R_b as shown in Table 6 and also shown in Fig. 17 as a function of y_{hem} cut.

	ΔR_b	ϵ_{uds}	ϵ_c	$C_b - 1$
Default MC		0.00077	0.01145	0.00001
$g \to c\bar{c}$ on uds only	-0.00070	0.00113		
$g \to c\bar{c}$ on uds, c background	-0.00094	0.00113	0.01189	
$g \to c\bar{c}$ on uds, c and correlations	-0.00097	0.00113	0.01189	-0.00012
$g \to b\bar{b}$ on uds only	-0.00041	0.00098		
$g \to b\bar{b}$ on uds, c background	-0.00053	0.00098	0.01167	
$g \to b\bar{b}$ on uds, c and correlations	-0.00052	0.00098	0.01167	0.00000

Table 6: Detailed breakdown of $g \to Q\overline{Q}$ effects for 97-8 R_b measurement.

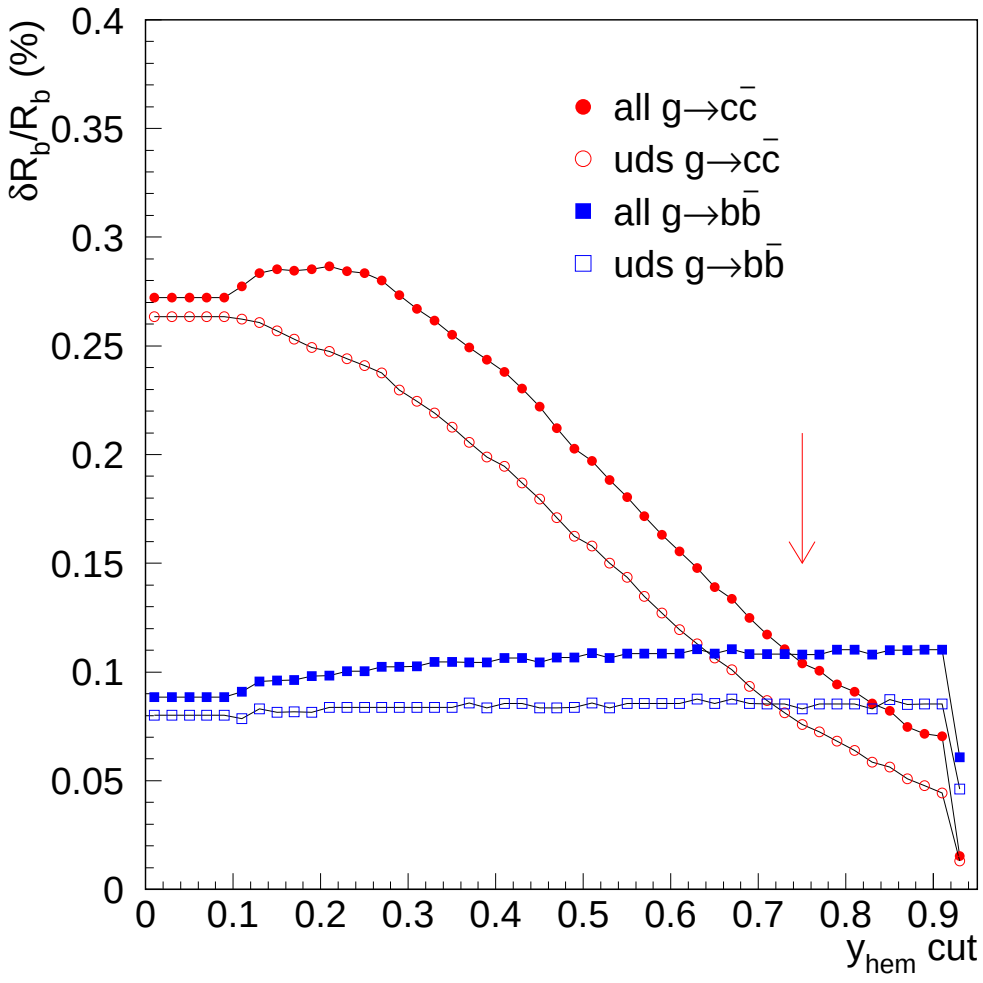

Figure 17: R_b systematic error as a function of flavor separation y_{hem} cut for the various $g \to Q\overline{Q}$ components.

These corrections are clearly quite large (c.f. the R_b statistical error is ± 0.00094). The uncertainty on $g \to c\overline{c}$ ($g \to b\overline{b}$) is $\sim$24% (46%) of the central value corrections. The $g \to b\overline{b}$ rate is measured by several experiments with very comparable results, while $g \to c\overline{c}$ is primarily based on just the OPAL measurement with a quite tight error. The reliability of the $g \to c\overline{c}$ correction is therefore not as solid. Unfortunately, the signatures of $g \to c\overline{c}$ and glubb are not very distinct compared to the normal $c\overline{c}$ and $b\overline{b}$ as seen in Fig. 18

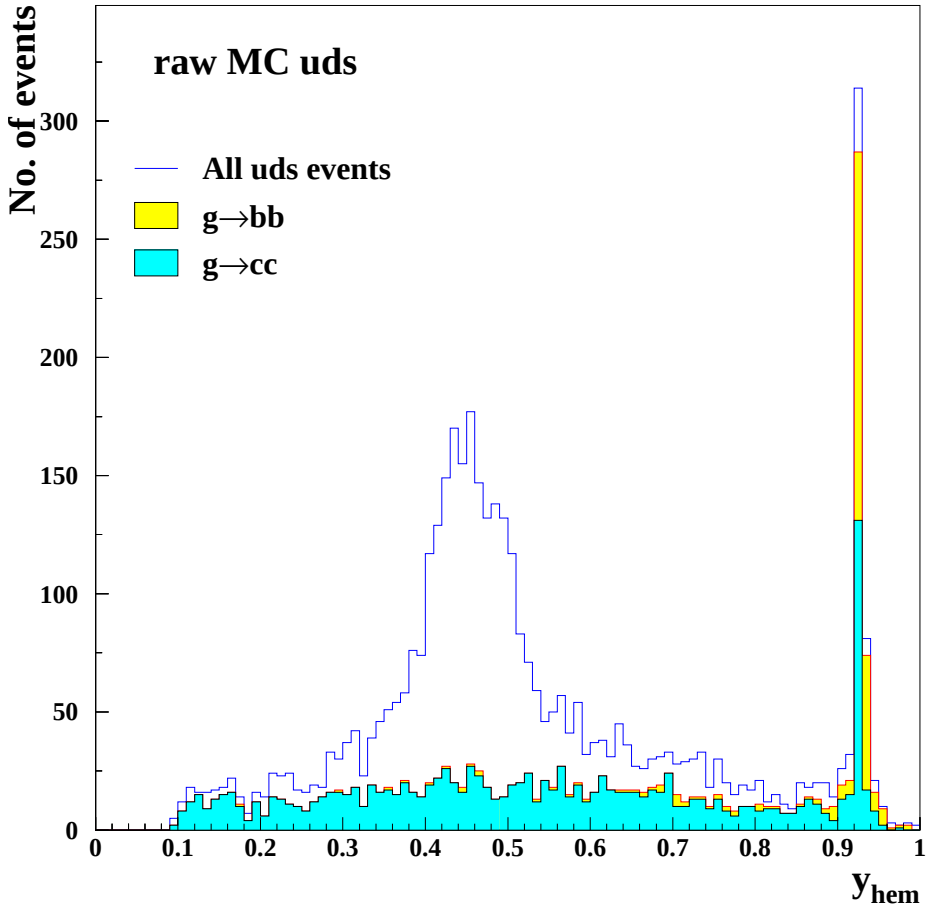

Figure 18: MC *uds* hemisphere tag NN flavor separation variable y_{hem} and the $g \to Q\overline{Q}$ components.

The *uds* mis-tags are dominated by $g \to c\overline{c}$ for low y_{hem} charm tag, a mixture of $g \to c\overline{c}$ and $g \to b\overline{b}$ for the high y_{hem} b-tag. Given that the raw MC $g \to Q\overline{Q}$ rate is low by a factor of two. The actual fraction of $g \to Q\overline{Q}$ should be even higher. Given this irreducibility, higher precision R_b measurements at statistics equivalent to a few times SLD or more, must go hand in hand with the $g \to Q\overline{Q}$ measurements.

5.2.2 *uds* physics modelling

Among the fake *uds* tags, a significant fraction involve the K_s^0 and Λ decay product. The MC generator level K_s^0 and Λ production are varied by $\pm 10\%$, as recommended in [17], to derive the systemtic uncertainty due to light hadron production.

5.2.3 charm production and decay modelling

The charm production and decay modelling affect the R_b, R_c measurement through the uncertainty on the small charm tagging efficiency in the b-tag. They also affect the R_c measurement through the charm tag hemisphere correlations. Many of the production and decay uncertainties only affect charm tag correlations indirectly, e.g. through the primary vertex reconstruction.

The different charmed hadrons have very different lifetimes and also rather different decay multiplicities so that the tagging efficiencies are also rather different. The D^0, D^+, D_s and Λ_c lifetimes are varied according to their measured values as in PDG. The production fractions of these different charmed hadrons are varied according to the measured values at LEP [17].

The tagging efficiency is in general higher for higher momentum charmed hadrons so that the energy spectrum of the charmed hadrons is another source of uncertainty. Charmed hadron fragmentation is studied by varying the average scaled energy in the range $\langle x_E \rangle = 0.484 \pm 0.008$ using the Peterson fragmentation function [19], as well as by comparing the difference between the Peterson and Bowler models [20] for the same values of $\langle x_E \rangle$.

Charm tagging efficiency has a sensitive dependence on the decay charged multiplicity. The fraction of decays with less than two tracks are obviously crucial sources of inefficiencies. Higher multiplicity verticies are easier to identify, but the softer decay product momenta do not necessarily make the vertex resolution etter. The uncertainty due to D decay charged multiplicities are estimated by varying each decay multiplicity fraction according to the Mark-III measurement errors [21], for D^0, D^+ and D_s in turn, with a specific scheme as described in [17].

The production of K^0 in charm decays is another relevant source of uncertainty, although may be somewhat correlated to the charged multiplicity. In the case of K_L^0 or all neutral K_s^0 decays, it is a significant source of charged multiplicity loss. In the case of $K_s^0 \to pi^+\pi^-$ of decays, its decay product may interact with the vertexing of charm decay differently depending on the K_s^0 decay length. There is no explicit recommended scheme from LEPEWWG. We reweight the charmed hadron decay K^0 mutiplicity to correspond an average multiplicity uncertainties consistent with the Mark-III measurement [21].

Charmed hadron decays with fewer neutral particles have higher charged mass and are therefore more likely to be mistagged as a b. Thus, an additional systematic uncertainty is

estimated by varying the rates of charmed hadron decays with no π^0's by $\pm 10\%$. This is an SLD specific estimate with particular relevance to mass tags, while this is typically not included in LEP measurements.

The SLD MC charm production and decay simulation are not exactly the same as the LEPEWWG recommended central values. For the R_b measurement we previously didn't correct the central values for this difference and now two of the more significant ones are corrected: a) $c\overline{c}$ charm hadron production species reweighting to the recommended values corresponds to $frac\delta\epsilon_c\epsilon_c = +0.5\%$ at the nominal $y_{hem} > 0.75$ b-tag cut; b) D decay charged multiplicity distribution reweighting to MK-III measurement, corresponds to $frac\delta\epsilon_c\epsilon_c = -2.5\%$. The discrepancy in the MC is primarily due to D^+ 1-prong decay BR in the simulation is considerably lower than the MK-III data. The combined effect is a correction of $\Delta R_b = +0.00012$, which is a small fraction of the R_b statistical error.

An interesting check is to examine the various R_b physics systematic contributions for c and uds as a function of the y_{hem} cut sweeping through very different b purity ranges as shown in Fig. 19. This plot is for illustrating the basic trend, while it is actually from the Summer-00 analysis for 97-98 data using only the all flavor MC. The current result is based on Summer-01 analysis including $c\overline{c}$ MC is slightly different, but within MC statistics. Also to note is that the gluon splitting systematics plotted was only the major component which affects uds efficiency. The general trend of reduction as y_{hem} increases is as expected. The dip of uncertainty for the $c \to D_s + X$ at y_{hem} cut of $\sim$0.2 could be a coincidence that the tagging efficiency for D_s happened to be the same as the tagging efficiency of the remaining c-hadron mixture. Similarly, the uncertainty dip for $D^0 \to K^0$ at y_{hem} cut of $\sim$0.25 could be due to a lucky balance of D^0 decay modes with/without K^0 having the same efficiency at that cut. The almost flat $g \to b\overline{b}$ component for uds systematics is just another perspective of Fig. 18 where the $g \to Q\overline{Q}$ events are known to also cluster at very high y_{hem}.

5.2.4 b production and decay modelling

The b hadron production and decay modeling uncertainties only enter via the b-tag hemisphere correlation. Since the B decays, and to a large extent the b jet fragmentations proceed independently between the two hemispheres, most of these effects (apart from the QCD gluon radiation effect discussed separately in the next section) enter indirectly through e.g. primary vertex reconstruction.

The b-hadron lifetimes are varied by a typical current measurement error of ± 0.05ps. We also vary the Λ_b production ratio (outside the LEPEWWG recommendation) by current measurement uncertainty to acknowlege the fact that the Λ_b lifetime is significantly shorther than the B mesons. b hadron fragmentation is studied by varying the average scaled energy in the range $\langle x_E \rangle = 0.702 \pm 0.008$ using the Peterson fragmentation function [19], as well as by comparing the difference between the Peterson and Bowler models [20] for the same values of $\langle x_E \rangle$. The B decay charged multiplicity distributions are reweighted to correspond an average charged multiplicity uncertainty of ± 0.35.

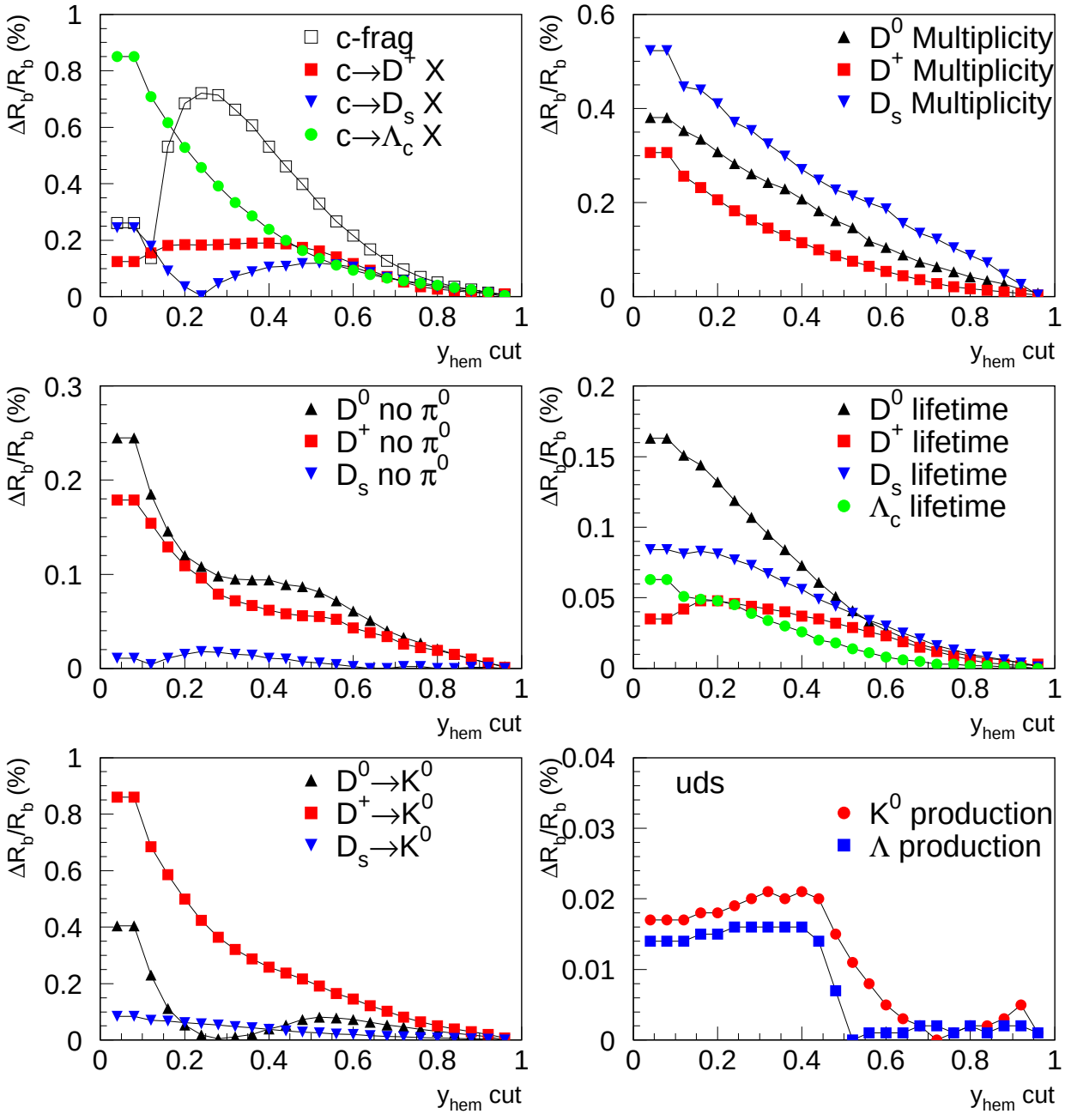

Figure 19: R_b systematic for various physics sources on *uds* (bottom right plot) and $c\bar{c}$ (other 5 plots) background as a function of y_{hem} cut, for 97-8 analysis. Note that the vertical scales for t he 6 plots are different.

Hemisphere type	b-tag efficiency	c-tag efficiency
Normal hemispheres with one heavy hadron	0.634	0.231
Two heavy hadrons in same hemisphere	0.647	0.166
hard gluon hemisphere	0.015	0.008

Table 7: b/c-tag efficiencies for different types of hemispheres in MC $b\overline{b}$ and $c\overline{c}$ events.

5.2.5 Gluon radiation effects on tag correlations

Gluon radiation is a more direct source of correlation as it tends to simultaneously lower the momenta of both heavy quarks as well as changing their directions from the back to back topology. The tags are generally sensitive to heavy hadron momentum and their directions w.r.t. the thrust axis.

We first discuss the extreme case of a very hard gluon radiation which causes two heavy hadrons recoiling into the same hemisphere, which creates an anti-correlation of tagging efficiencies between the two hemispheres. Hard gluon radiation resulting two B's in the same hemisphere is happening at a rate of 1.62% in the $b\overline{b}$ MC passing the analysis event selection (generator level without event selection is 2.45%). Using both all flavor and $b\overline{b}$ MC from 97-98 with no detector corrections, the tagging efficiencies for the different types of hemispheres in b events are examined as shown in Table 7. Similarly, the same issue is also examined for a representative c-tag of $y_{hem} < 0.4$ for 97-98 $c\overline{c}$ MC which are also tabulated in Table 7. In the case of the b-tag, the two B's in the same hemisphere is actually largely compensated by the lowering of B momentum and wider angles to the thrust axis so that the b-tag efficiency is only slightly higher than a normal single b hemisphere. However, in the case of the c-tag, the reduced c-hadron momentum and the more confusing kinematic situation actually turned out to be a larger effect to make the two c-hadron hemisphere even having a significantly lower efficiency than normal. In the case of a small hard gluon fraction of f_{2H}, and with a simplified model of gluon tag efficiency=0, we have $\Delta C \sim f_{2H}(1-\epsilon_{2H}/\epsilon_{1H}-f_{2H})$ where ϵ_{2H} and ϵ_{1H} are the tag effciencies for hemisphere with two heavy hadrons and the normal one heavy hadron respectively. In the b-tag case of ϵ_{2H} and ϵ_{1H} being very similar, a lucky cancellation occurs to make the sensitivity to hard gluon radiation much reduced. In the case of the c-tag, the fact that $\epsilon_{2H} < \epsilon_{1H}$ would in fact bring a positive correlation change instead of a large negative correlation one would naively associate with these hard gluon radiation events. The effect for adding the hard gluon events to MC without them is to result in $\Delta(C_b - 1) = -0.00037$. There is an actual analysis measuring the two B's in same hemisphere rate in Tom Wright's thesis [16] (Appendix B.4.1). This is done with a different event selection and b-tags applied to each jet in 3 jet events. This analysis measured the ratio of same hemisphere $b\overline{b}$ rates between data and MC to be 0.82±0.09. For the actual systematic uncertainty, we still conservatively follow the LEPEWWG recommendation to vary MC by ±30%, which results in a rather small error of $\delta R_b = -0.00002$. In the case of the R_c analysis, the hard gluon events in both $b\overline{b}$ and $c\overline{c}$ are weighed up by 30% for all tags

and the joint effect of $\delta R_c = +0.00026$ with the dominant effect coming from hard gluons in $c\overline{c}$ events.

Systematic error is also assigned to effects of heavy hadron momentum correlation between the two hemispheres, mostly due to soft gluon radiation and fragmentation effects, which in turn translate to a tagging efficiency correlation. In the case of B momentum correlation in $\overline{b}$ events, this is estimated by comparing the B momentum correlation in the HERWIG [22] and JETSET [10] event generators. At parton level, all generators give similar correlation of $\sim$1.4% between the b quarks. At hadron level, the correlation coefficient for the b-hadron momenta in the two hemispheres is 1.55% in JETSET, while the largest deviation among different models is seen in HERWIG which gives up to +0.8% higher B momentum correlation. The LEPEWWG's recommendation is to use half of this difference of 0.4% as the variation to estimate systmatic error. Given that different event selections can change the absolute correlation (excluding case of two B in same hemisphere, JETSET correlation reduces to 1.23%, and applying $N_{jet} < 4$ cut further reduces this to 0.85%), the ratio of 0.4%/1.55%=26% is taken as the fractional uncertainty on the b momentum correlation effect. There is an actual analysis of B hadron energy correlation in Tom Wright's thesis [16] (Appendix B.4.2) using the observed vertex momentum in double tagged events. The B momentum correlation observed is in good agreement with MC to at $\pm$20% level. The component of b tagging corrrelation due to B momentum correlation is estimated to be corresponding to $C_b - 1 = 0.00107$, as described in section 5.1, which translates to an error on R_b of 0.000060. There is no equivalent recommendation for c-hadron momentum correlation in $c\overline{c}$ events, mainly because this is only relevant for double tag analysis which is not done at LEP. We similarly take 26% of the D-momentum correlation component in $c\overline{c}$ correlation (see Table 5.1) as a systematic uncertainty, which corresponds to $\delta C_{c-tag} = 0.0020$ and δR_c of 0.00022.

5.3 Detector systematics

5.3.1 Tracking resolution and efficiency

The tracking resolution systematic effects, primarily due to residual detector misalignment is estimated from the observed shifts in the track impact parameter distributions as a function of ϕ and θ in both r-ϕ and r-z planes. The typical impact parameter biases observed in the data are $\sim 2.5\,\mu$m ($\sim 5\,\mu$m) in the r-ϕ (r-z) plane. A correction procedure is applied so that the MC tracks match the mean bias values of the data in various (ϕ, θ) regions. This is a more realistic evaluation of alignment bias effects, where tracks passing the same detector region are biased in a correlated manner. The actual corrections are implemented by dividing ϕ into 40 regions according to VXD3 ladder triplet boundaries and 4 sections in θ. A detailed description of the resolution corrections can be found in Aaron's thesis [13] (chapter 3). Half of this correction is taken as the variation to evaluate the track resolution systematic error.

The uncertainty in the tracking efficiency is evaluated from a comparison between data and MC for the fraction of all CDC tracks which pass a set of quality cuts, and the fraction

	R_b	$\epsilon_b(\%)$	$\epsilon_c(\%)$	$\epsilon_{uds}(\%)$	$C_b - 1$
Raw base values	0.21925	62.911	1.136	0.0733	0.00042
Statistical error	0.00104	0.034	0.009	0.0027	0.00047
Corretion effects	δR_b	$\delta\epsilon_b(\%)$	$\delta\epsilon_c(\%)$	$\delta\epsilon_{uds}(\%)$	δC_b
Only resolution corr.	-0.00041	-0.073	$+0.055$	$+0.0051$	-0.00007
Only tracking eff. corr.	$+0.00026$	$+0.012$	-0.043	-0.0022	$+0.00002$
Both res. and eff. corr.	-0.00022	-0.059	$+0.009$	$+0.0041$	-0.00041

Table 8: Effect of the tracking corrections on parameters in the R_b analysis. The base values of the various parameters are raw values from uncorrected MC before any corrections as a magnitude reference.

of good CDC tracks extrapolating close to the IP that does not have associated VXD hits. These studies indicate that the MC overestimated tracking efficiency by $\sim$1.5% on average. A procedure for the random removal of tracks in bins of p_t, ϕ, and θ is used to correct the MC for this difference. We were previously unsure whether the track efficiency correction is really correcting real tracking inefficiency or possible MC generator over-production of tracks. Secondary vertex charge distributions are used as an independent check to verify the width of the vertex charge distributions agree better between data and MC with these corrections applied, as shown in Fig. 20. The $c\overline{c}$ MC is reweighted to the the nominal LEPEWWG charm hadron production fractions.

This is a considerably better test, directly on the secondary vertex tracks we care about and independent of the fragmentation track multiplicity which is harder to know what to expect. The vertex summed charges are only supposed to be 0 or ± 1 for perfect reconstruction so that even the dependence on decay multiplicity only comes in at second order. There is still some physics model coupling as to the charged/neutral heavy hadron production ratio, but the bins with $|Q| > 1$ are mostly sentitive to real tracking efficiencies. The resolution corrections have rather small effect on the vertex charge so that most of the tracking corrections effects here are from the tracking efficiency corrections, which is clearly bringing a better agreement between data and MC. Given that we are now more confident that the track efficiency correction is doing what expect, half of the full correction is used as a variation to derive the tracking efficiency systematic errors (we used to quote the full correction as systematic). There is a similar test in Tom Wright's thesis [16] with similar conclusion. This check is slightly different from the vertex charge A_b, A_c analysis in Tom Wright's thesis: a) slightly different tag y_{hem} cuts; b) The A_b, A_c analysis also used VXD3 alone vectors to improve the charge reconstruction. This check is using exactly the vertexing output for this analysis.

To quantify the effect of the tracking corrections in some detail, the changes of various quantities due to the application of the tracking corrections are tabulated in Table 8 for the R_b measurement. Most quantities exhibite the expected behavior that combining both corrections is close to be just the linear sum of the two corections separately. However, the correlations can fluctuate at one MC statisitcal σ level. The variations of tagging efficiencies

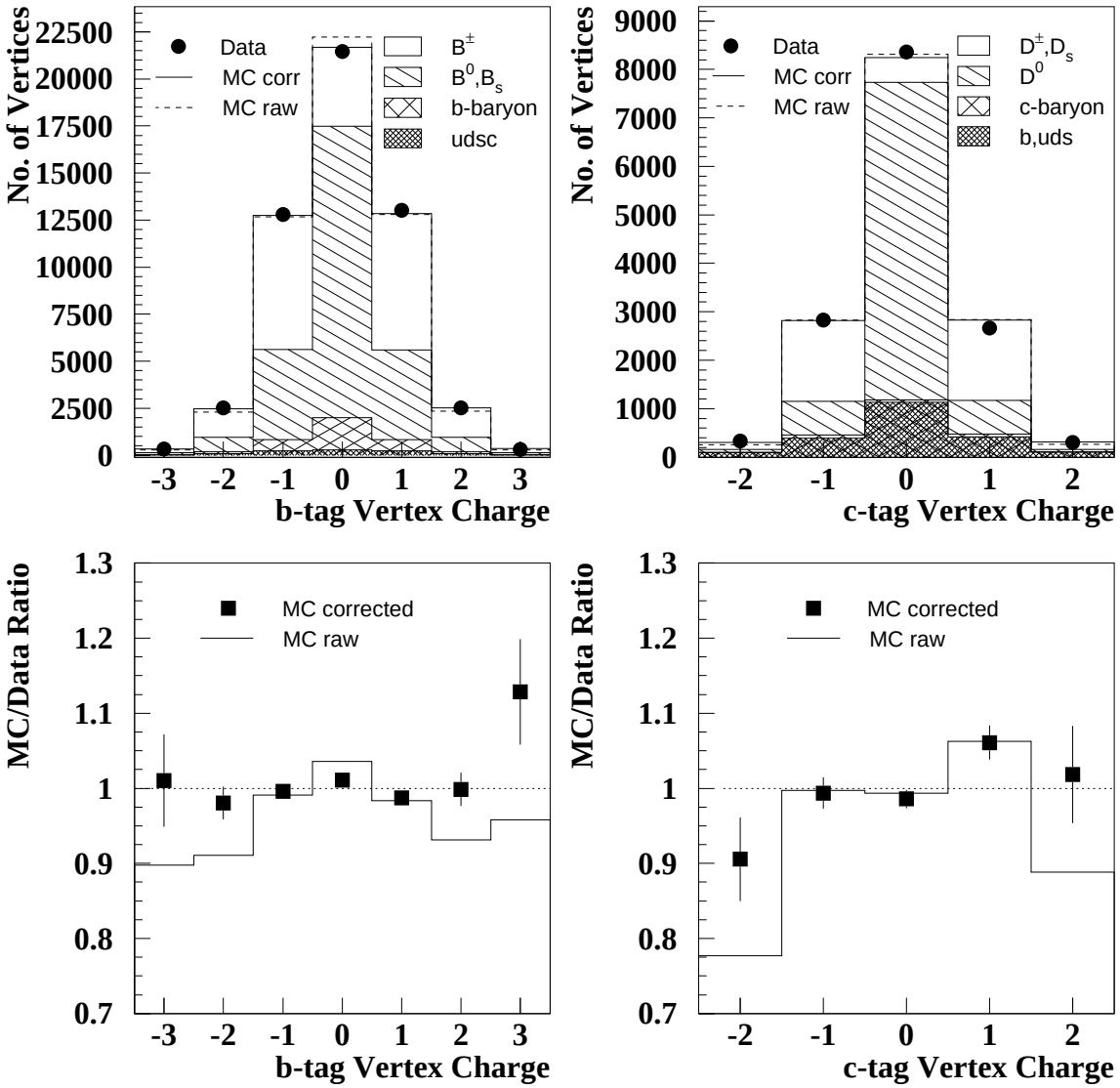

Figure 20: Vertex charge distributions for $y_{hem} > 0.75$ b-tag and $y_{hem} < 0.4$ c-tag hemispheres compared between data and MC with or without tracking corrections. The edge bins include underflow and overflow vertex charge entries.

and tag correlations are also plotted as a fucntion of the minimum y_{hem} cut in Fig. 21 and Fig. 22.

5.3.2 IP tail

Another potential systematic source is the possible tails in the IP position determination which can cause large tagging asymmetries. The lower statistics $Z^0 \to \mu^+\mu^-$ events have no indication of systematic tail effects. A further study (details in Sean Walston's thesis) [23] is done by examining the 'YT' distribution of the distance between the hemisphere axis drawn through the fitted event primary vertex in $r-\phi$ to the IP for 2-jet hadronic events with no secondary decay tracks. This was used previously in Mark-II and early days of SLD VXD2 by Steve Wagner as a IP resolution and tail analyser with higher statistics than lepton pairs. The difficulty with studying the IP resolution is that it's hard to find high enough resolution probes which can measure it. The basic idea of the YT distribution is to look at the IP resolution in the direction perpendicular to the jet direction to get the best resolution, i.e. the 'impact parameter' of a jet. The requirement of all quality tracks fit into the primary vertex with good χ^2, largely remove the b, c events to obtain a uds sample at >95% purity. The comparison of between data and MC for the IP tails are shown in Fig. 24.

There is no significant discrepancy between data and MC for 97-98 data, but there is a detectable tail in the 96 data with $\sim$100 μm width for 0.5% of the event. The full effect of the tail is treated as a systematic for the 96 data.

For the tag correlations, there is also some concern of on the reliability of the thrust axis simulation. A cross check is performed by looking at the separation angle between well reconstructed b-tag vertices and its hemisphere thrust axis. The vertex direction is defined geometrically by the vertex position and PV. A comparison between data and MC is shown in Fig. 25. The widths of the angular separations are actually reasonably simulated by the MC, given the complicated fragmentation modelling involved. There is a detectable bias in θ as vertice tend to come out at shallower polar angles. There could be some bias in the KAL thrust direction as energy measurements are degraded at 45° gap and endcap regions. Whatever it is, the MC is simulating the bias already. In ϕ, it looks like we have some uncrrected rotation between KAL and CDC. However, this is a rather small rotation. Running the analysis with the rotation correction had negligible effect so that no additional systematic is assigned.

5.3.3 Geometric and temporal correlation effects

Besides the issue of overall tracking efficiency uncertainty, MC modelling uncertainties on the efficiency nonuniformity due to significant local detector inefficiencies and time variation can lead to system uncertainties on tagging correlations. The contribution of the θ and ϕ tagging efficiency dependence to the overall tagging efficiency correlation are evaluated in section 5.1. We estimate the uncertainty of the MC modelling of θ and ϕ dependency, by compare the hemisphere tagging fractions between data and MC for the $y_{hem} > 0.75$ b-tag and representative $y_{hem} < 0.4$ c-tag. The comparison for tagging fractions as a function of hemisphere thrust $\cos\theta$ are are shown in Fig. 26 for 97-98 analysis, and in Fig. 27 for 1996

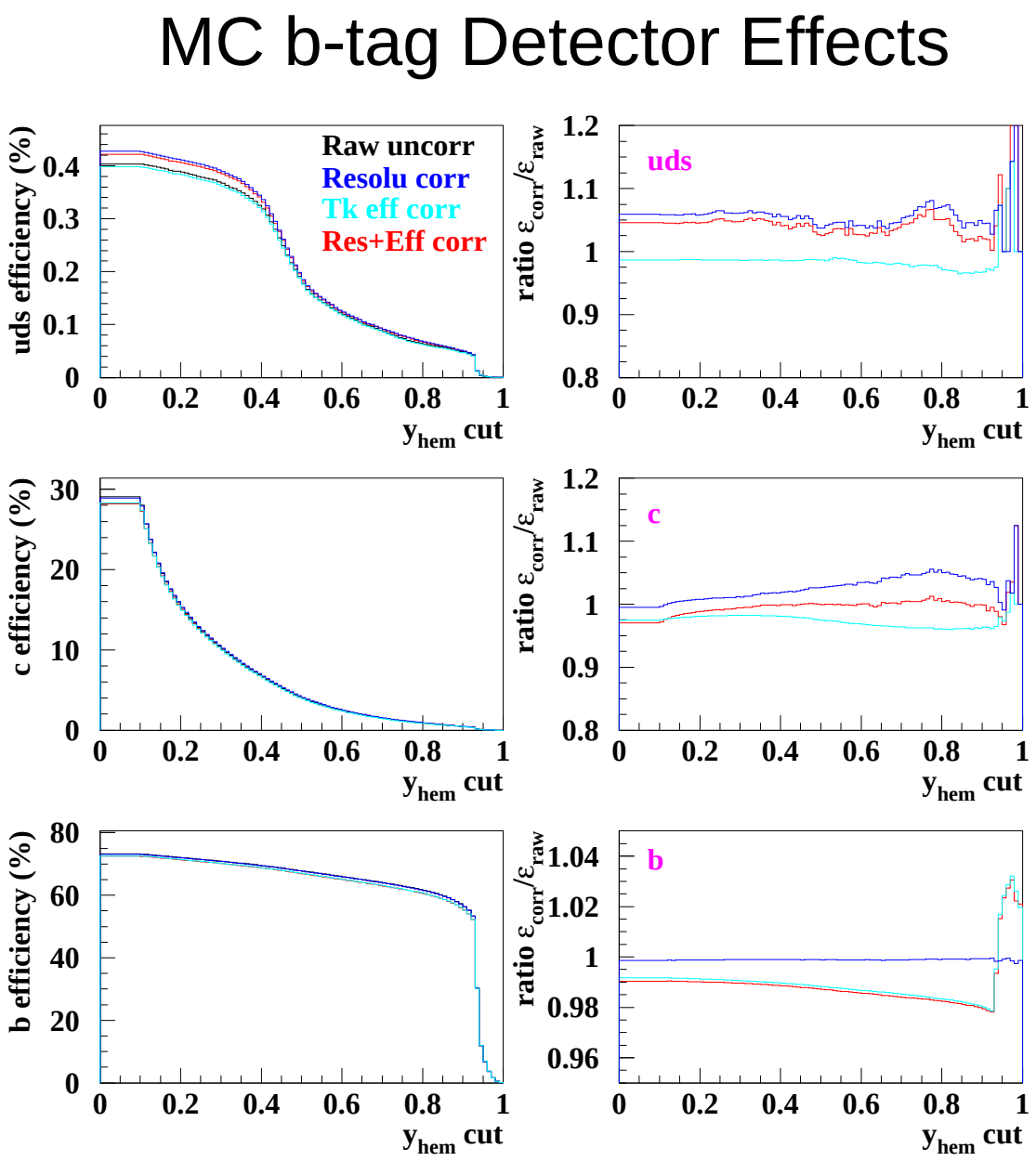

Figure 21: Effects of tracking corrections on tagging efficiencies as a function of miminum y_{hem} cut.

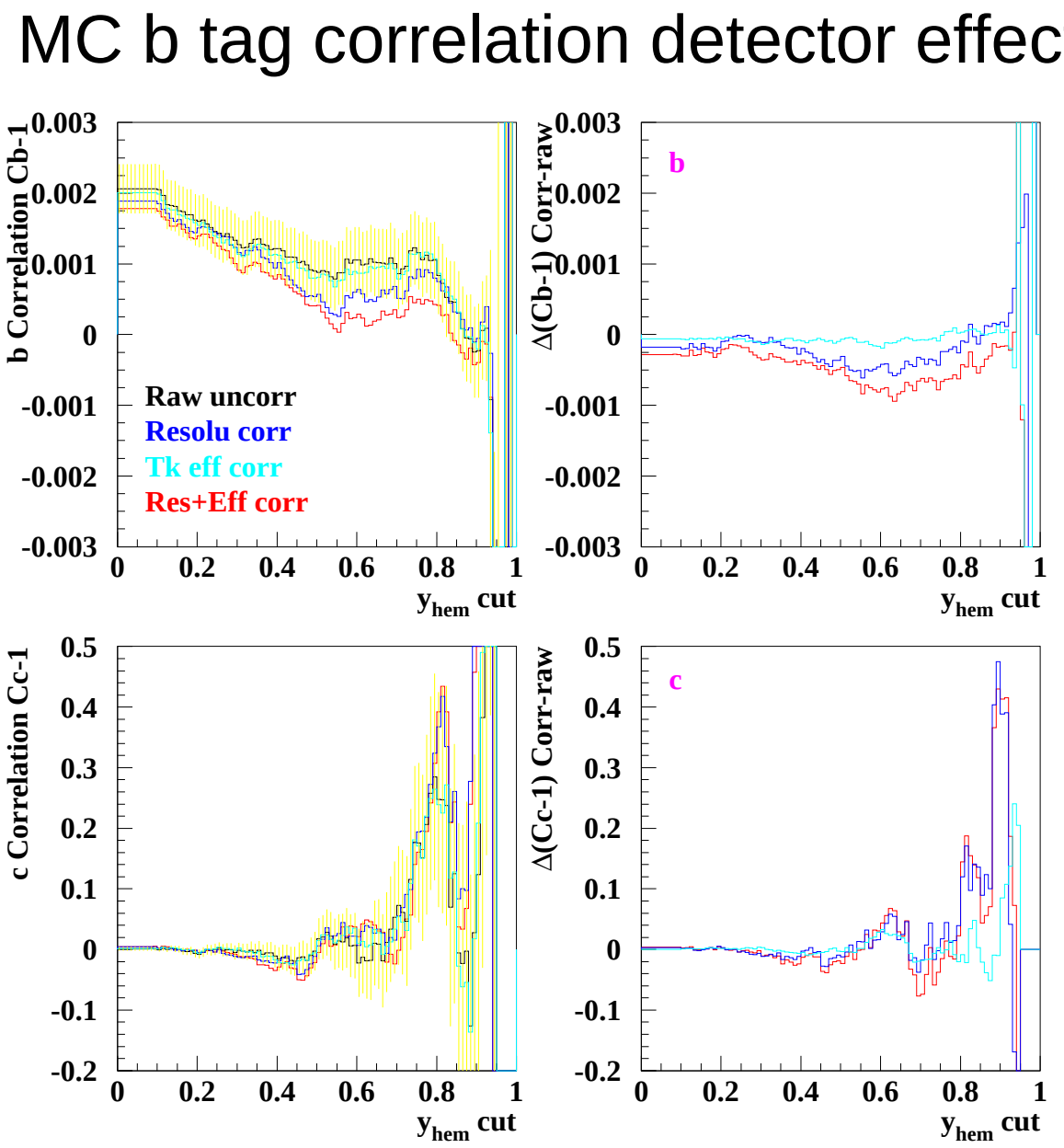

Figure 22: Effects of tracking corrections on tagging correlations as a function of miminum y_{hem} cut.

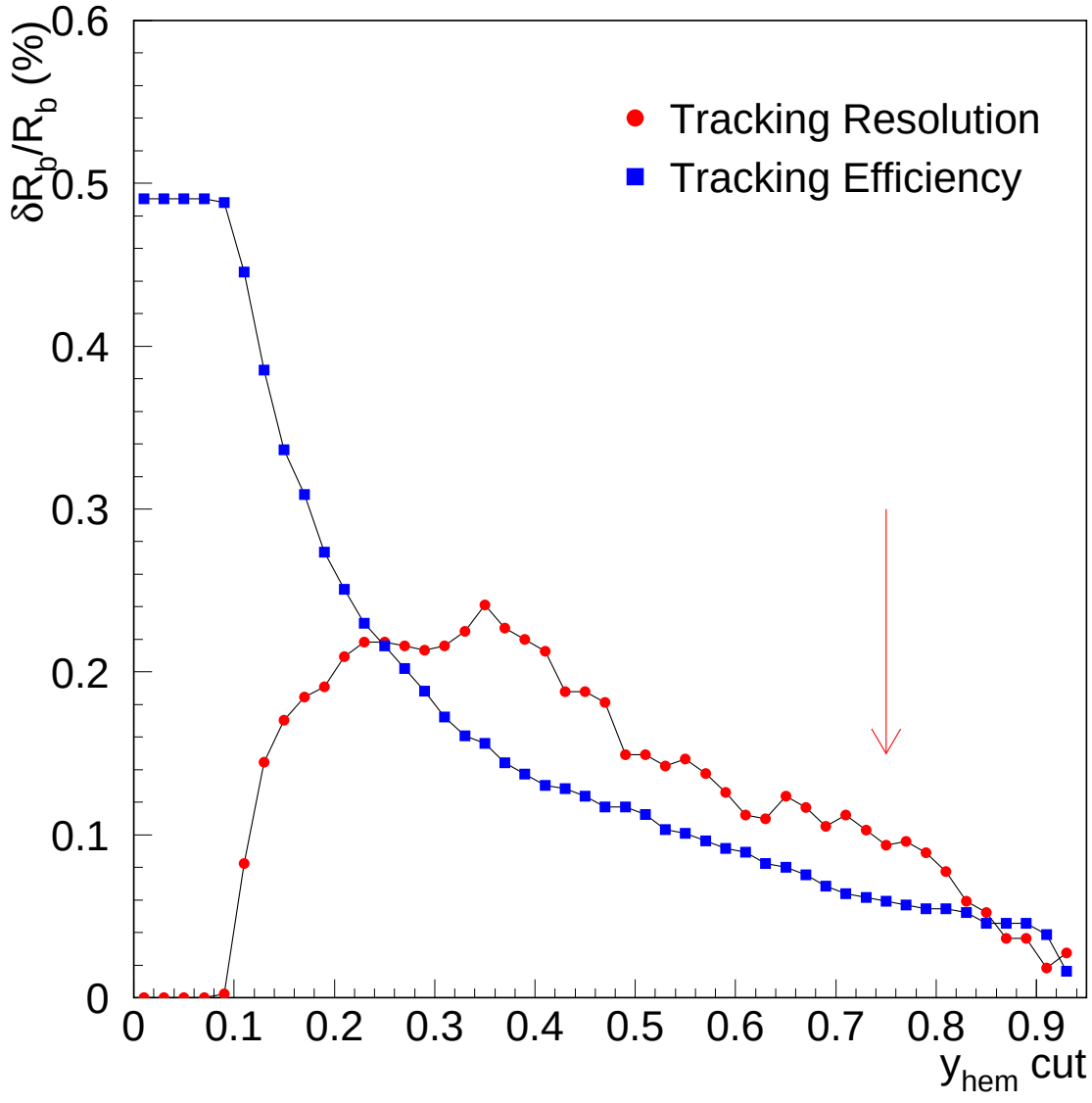

Figure 23: R_b systemics due to tracking resolution and efficiency uncertainty as a function of miminum y_{hem} cut, for 97-8 analysis.

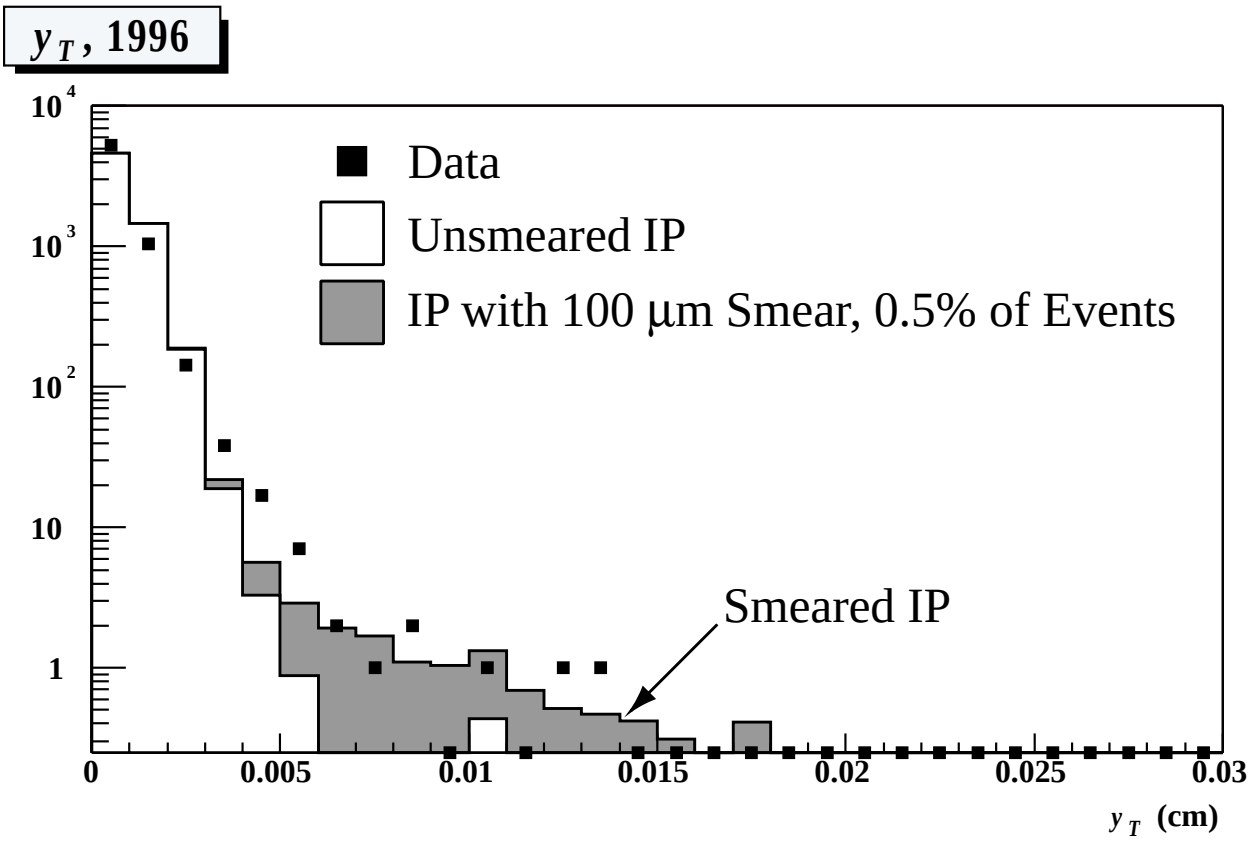

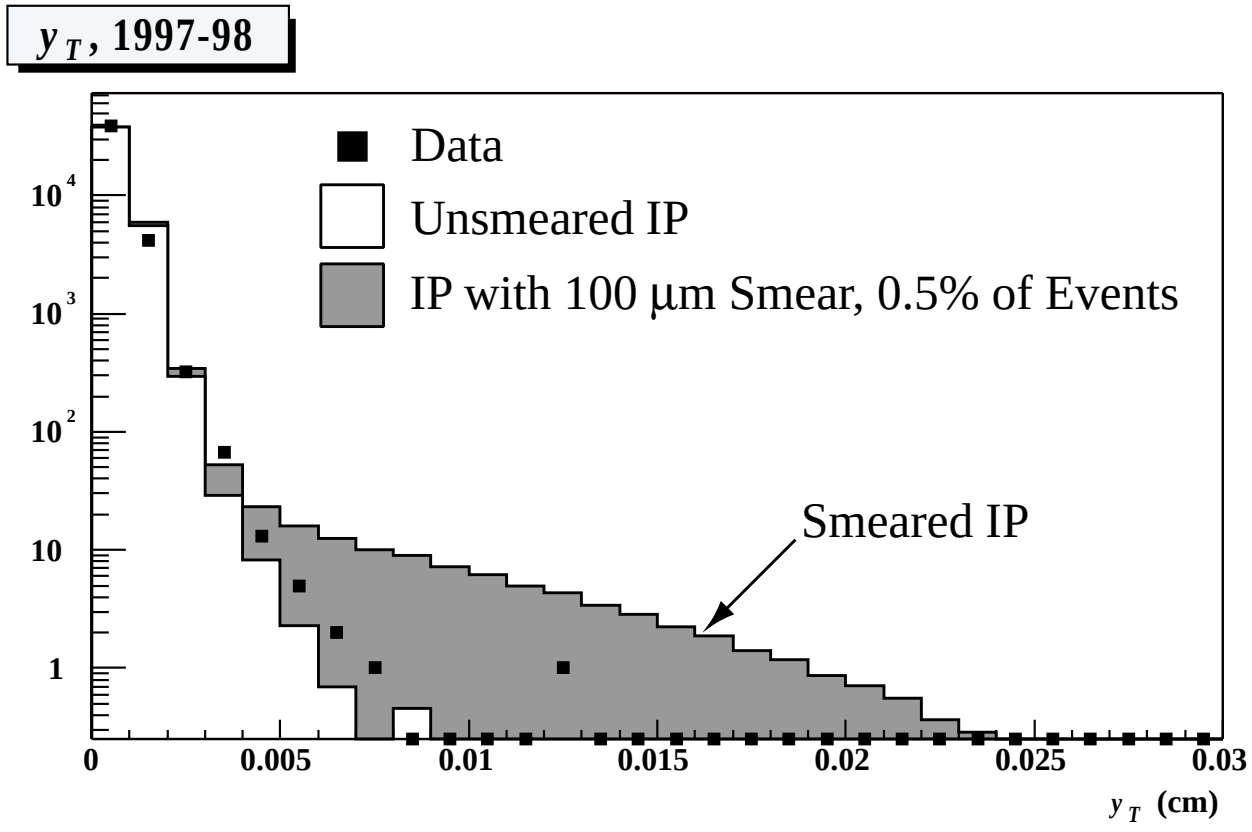

Figure 24: YT distributions comparing between data and MC for 97-98 and 96.

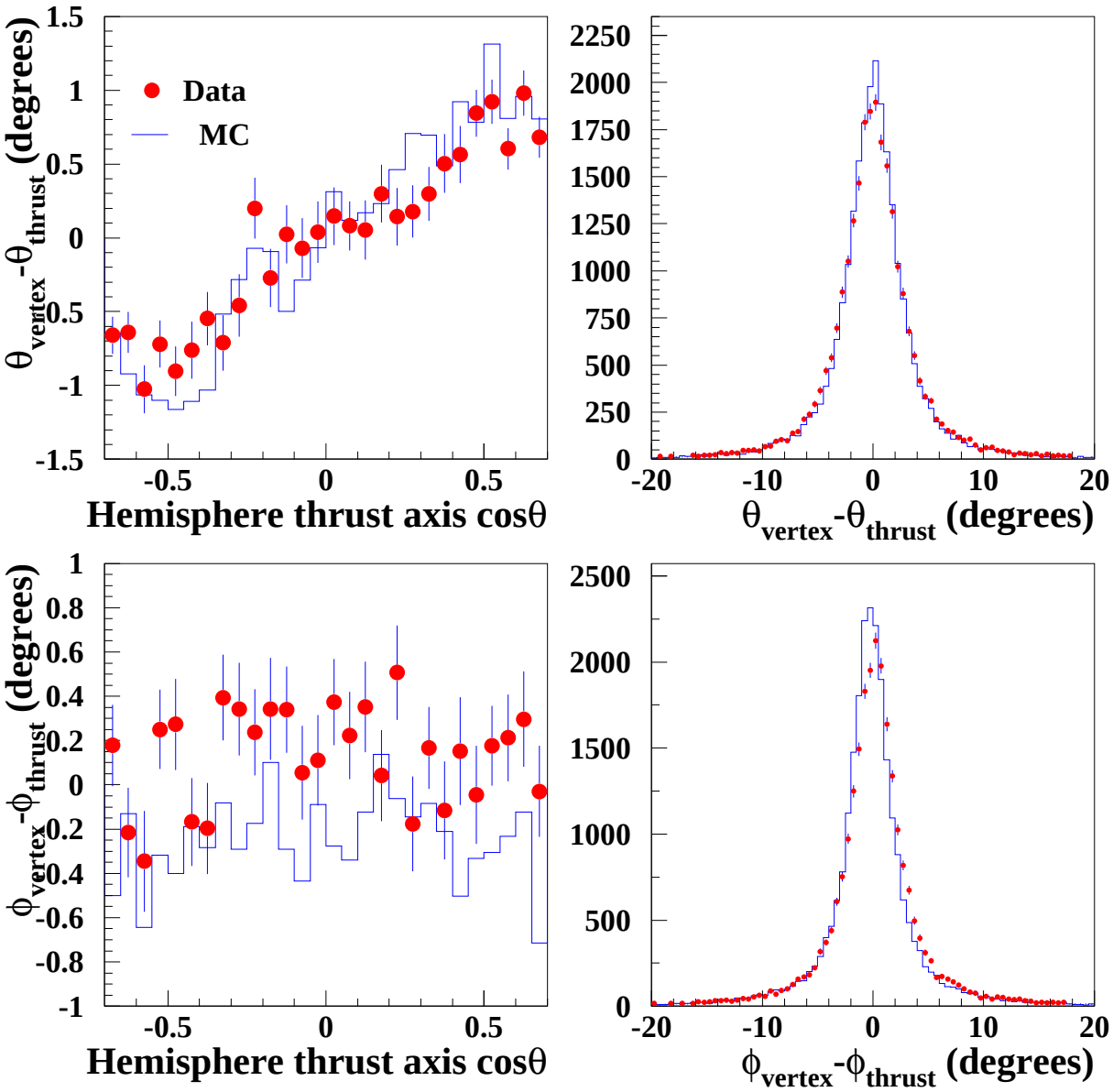

Figure 25: Comparison of angular separations between b-tag vertex and thrust axis between data and MC.

	ΔC_{b-tag}		ΔC_{c-tag}	
	97-98	96	97-98	96
θ effect	0.00016	0.00181	0.00043	0.00337
ϕ effect	0.00027	0.00037	0.00030	0.00409
time dependence		0.00029		0.00055

Table 9: Correlation systematic uncertainties due to geometrical and time dependent effects.

analysis. The corresponding comparisons for the b-tag as a function of the hemisphere axis ϕ are shown in Fig. 28 for 97-98 analysis, and in Fig. 29 for 1996 analysis. There is a generally good agreement between the data and MC within the statistical errors. The only significant effect is the variation in ϕ for 96 data, due to electronics failures for some of the periods, which is nonethless reasonably simulated by the MC. To estimate the correlation uncertainty, we simply take the ratio of the all input hemisphere tagging fractions between data and MC for each ϕ and θ bin, to reweight the MC true signal tagging efficiency for the corresponding bin, as an approximated deviation. The reweighted ϕ and θ dependent effeciencies are then used to recalculate the tagging efficiency correlation components as described in section 5.1. The change of the tagging correlation from the reweighting is taken as a systematic error. Note that correlation component calculations are insensitive to overall efficiency differences between data and MC which may enter in the reweighting, but only to dependency shape variations. The resulting systematic errors on the geometrical correlations are summarized in Table. 9. The correlation systematic error on ΔC_{b-tag} translates directly to the fractional error $\delta R_b/R_b$ on R_b, and the error on the representative c-tag of ΔC_{c-tag} translates approximately to the fractional error $\delta R_c/R_c$. The use of data vs MC ratio unfortunately introduces statistical fluctuations on the estimated correlation change. A toy MC study indicates that the statistical fluctution expected for e.g. for the ϕ effect estimate is $\sim$0.00009 for 97-98 b-tag and as large as $\sim$0.0031 for the 96 c-tag. Some of the changes are consistent with statistical fluctuation, but we still conservatively take them as systematic uncertainy.

For the time dependent effects on the tagging correaltions, there is a very good uniformity through out the large 97-98 sample so that the overall time dependence effect on tagging correlation is negligible and no extra systematic errors are assigned. The smaller 96 data sample does have significant time dependent effects spanning large fractions of the run periods, which contribute significantly to the overall correlation. Although this may not be obvious from the data and MC comparison previously shown in Fig. 2 due to large statistical errors, it is more apparent once combined runs in the middle period (Runs 34150-35050) to compare with the remaining runs. We take the ratio of the all hemisphere tagging fractions between the middle period to the rest of 96 and compare between data and MC. The fractional deviation between data and MC is translated into a systemtic error as the same fraction of the time dependence component of the correlation as estimated in section 5.1. The resulting systematic errors on the temporal correlations for the 96 analysis are summarized in Table. 9.

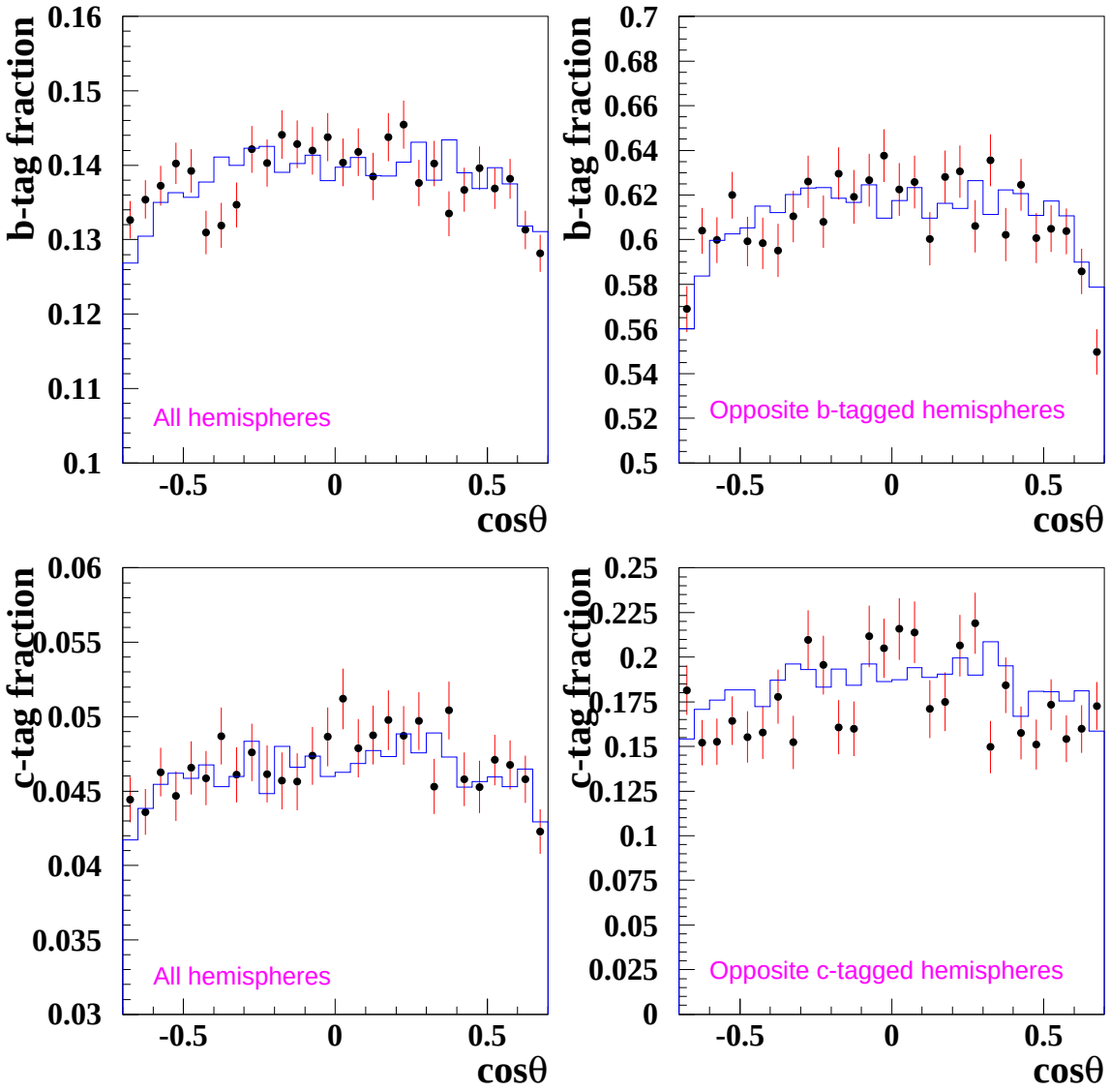

Figure 26: Comparison of 97-98 data (points) and MC (histogram) for b-tag and c-tag. The left column is for all input hemispheres and the right column is for the case that the opposite hemisphere is already tagged. Note the suppressed zero in vertical scale for the plots.

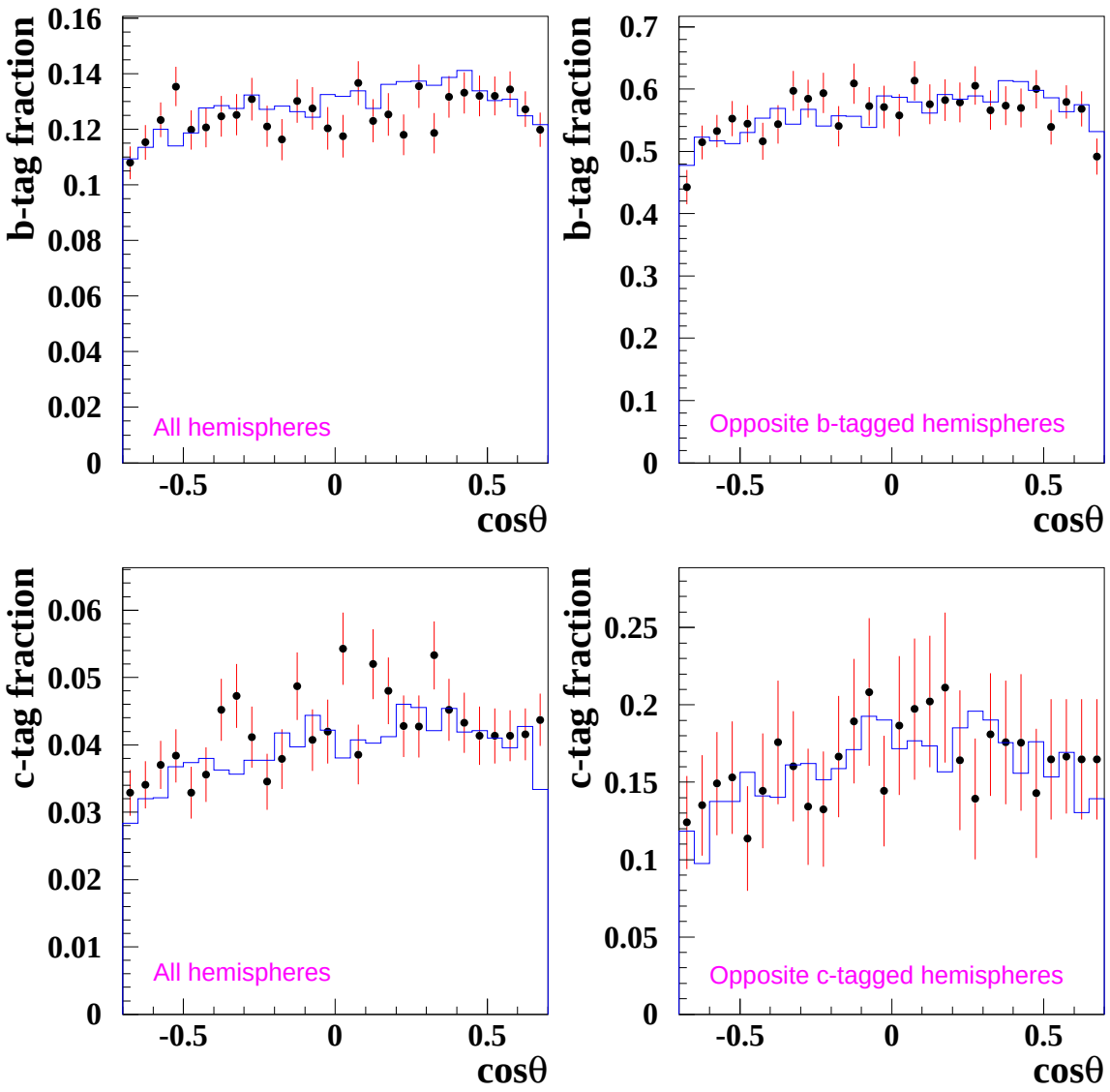

Figure 27: Comparison of 96 data (points) and MC (histogram) for b-tag and c-tag. The left column is for all input hemispheres and the right column is for the case that the opposite hemisphere is already tagged.

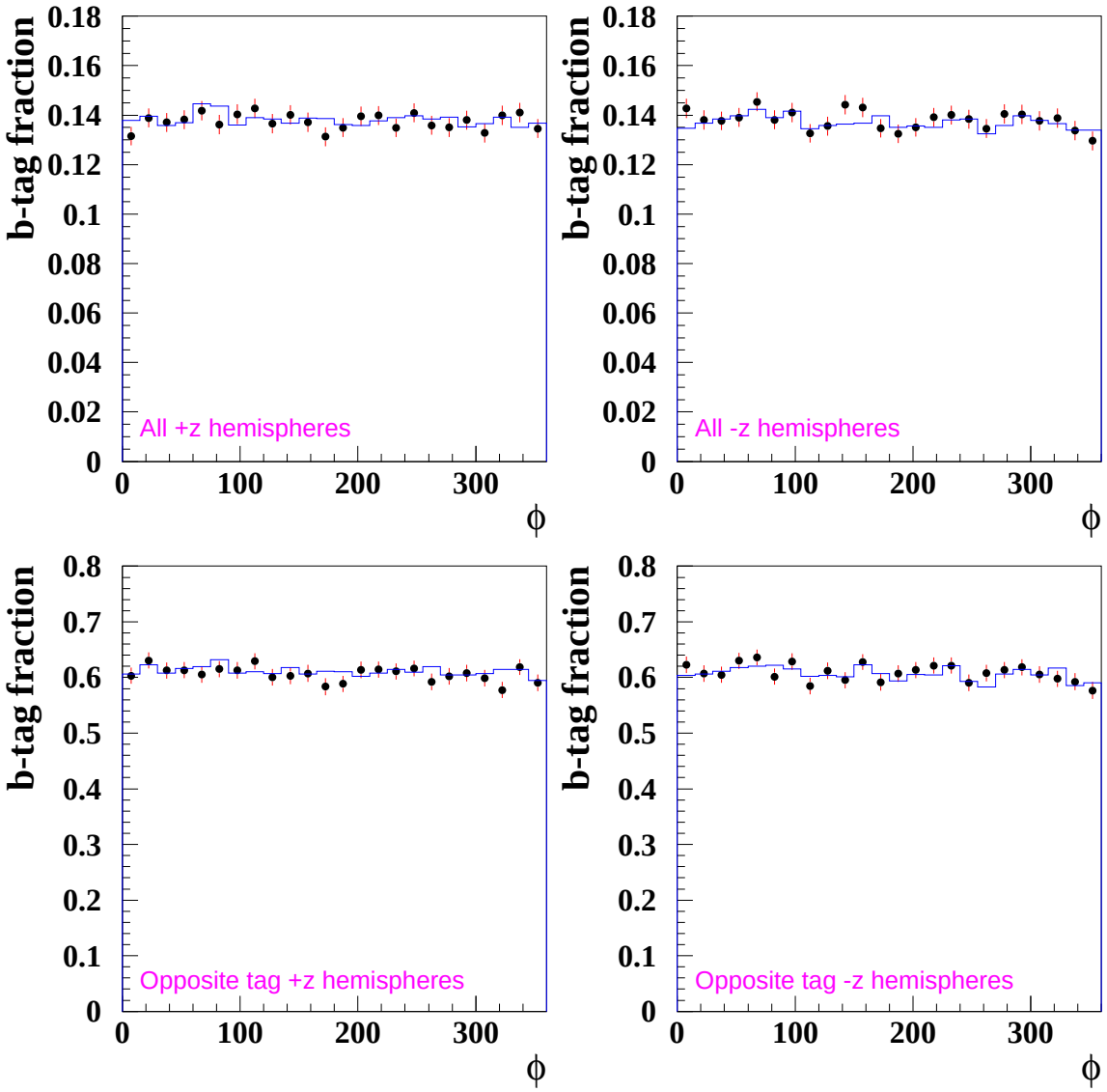

Figure 28: Comparison of 97-98 data (points) and MC (histogram) for b-tag. The top row is for all input hemispheres, with the *phi* variations examined for forward ($+z$) and backward ($-z$) hemispheres separately.The bottom row is for the case that the opposite hemisphere is already tagged.

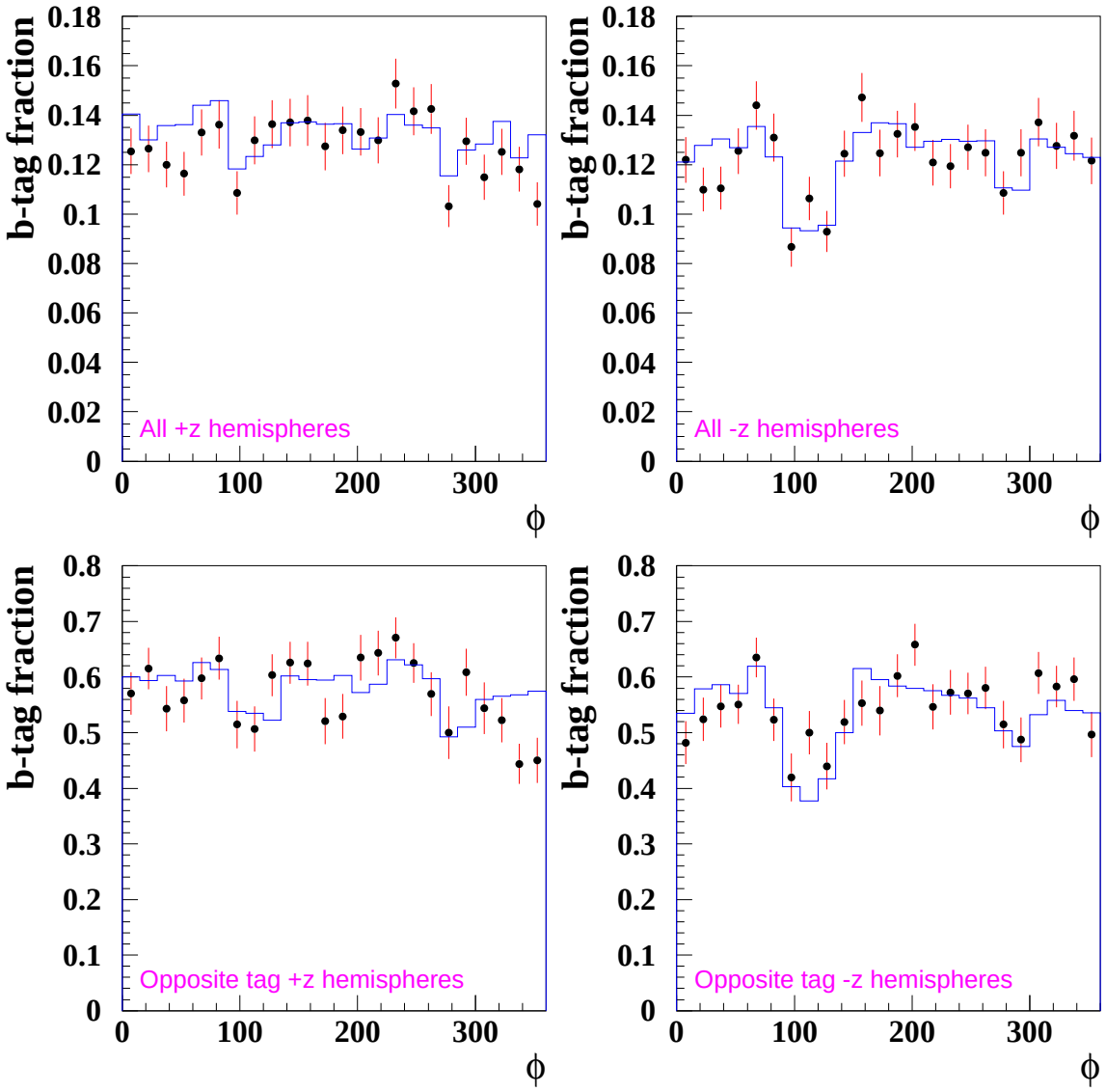

Figure 29: Comparison of 96 data (points) and MC (histogram) for b-tag and c-tag. The left column is for all input hemispheres and the right column is for the case that the opposite hemisphere is already tagged.

Stage	Basic Had. Sel.	$N_{jet} < 4$	Total
uds efficiency	$58.330 \pm 0.050\%$	$91.760 \pm 0.037\%$	$53.524 \pm 0.051\%$
c efficiency	$58.592 \pm 0.045\%$	$91.695 \pm 0.033\%$	$53.725 \pm 0.045\%$
b efficiency	$58.694 \pm 0.036\%$	$92.376 \pm 0.025\%$	$54.220 \pm 0.036\%$
ΔR_b	0.00089 ± 0.00016	0.00117 ± 0.00007	0.00207 ± 0.00017
ΔR_c	0.00040 ± 0.00018	-0.00035 ± 0.00008	0.00005 ± 0.00020

Table 10: Event selection flavor bias from the uncorrected 97-8 MC.

5.4 Event selection bias

The hadronic event selection flavor bias is evaluated from the MC for the basic hadronic event selection procedure and the last step of N_{jet} <4 cut separately. The basic selection includes trigger, pass 1 EIT filter and BBESEL with good detector period requirement. Given the reasonable matching of the MC production run periods for 97-98 all-flavor MC and $b\overline{b}$,$c\overline{c}$ only MC samples, we use all 97-98 samples to calculate the event selection bias. Since the relevant detector performance for hadronic selection is the same for 1996 data, we also use the same selection bias for the 96 analysis. The event selection efficiencies and resulting bias on R_b and R_c are tabulated in Table 10 The basic hadronic selection is passing a slightly higher fraction of $b\overline{b}$ events for the basic hadronic selection, which is expected from the known higher charged multiplicity and other observed kinematic differences of b-jets compared to uds. Given the effect is only a few σ, we simply take the MC statistical error as an uncertainty for this stage. The $N_{jet} < 4$ cut on the other hand is a more statistically significant effect while the rate of $c\overline{c}$ events passing the $N_{jet} < 4$ cut is consistent to be the same as uds (most of the ΔR_c is actually the compensating effect of R_b bias).

The effect of the b quark mass on ≥ 4 jet rate has significant theoretical uncertainty. Gluon radiation is suppressed for a massive b quark, but that suppression is not as large at high Q^2 due to the running b quark mass. The existing measurements of $m_b(m_Z)$ [24] based on 3 jet rates indeed give $m_b(m_Z)$ at $\sim$3 GeV/c^2.

In our previous attempts to evaluate the ≥ 4 jet cut bias, we assumed our production JETSET 7.4 MC being a proper representation of m_b=5 GeV/c^2 and just tried to correct the running m_b effect. However, through a very recent communication to Sjöstrand after our version 2 PRD draft release, he pointed out a important paper he wrote with his student in late 2000 [25] which we somehow missed completely. In this paper, they graciously documented the problems in gluon radiations from heavy quarks for older versions of JETSET/PYTHIA. In particular, starting from JETSET 7.4 and lasted until PYTHIA 6.129, the heavy quark gluon radiation suppression was overdone, with the 'dead cone' effect about a factor of two too large compared to data. The problem is explained in detail in sections 2.3, 2.4 of [25]. This excessive gluon radiation suppression was seen to clearly contradict the data used in the LEP/SLD running m_b measurements [24], as seen in section 5.1 of [25], especially for the 3-jet rate ratio between $b\overline{b}$ and uds, R_3^{bl}, in Fig.8 of [25]. This problem has a larger effect than the running b mass and needs to be corrected in addition.

We previously tried to vary the b quark mass in JETSET to estimate the effect of running

Source	Algorithm	Level	f_4^{uds} (%)	f_4^b (%)	R_4^{bl}
JETSET 7.4	`Yclus`	Parton	8.747±0.036	7.430±0.024	0.849±0.003
PYTHIA 6.228	`Yclus`	Parton	9.250±0.013	8.462±0.012	0.915±0.001
PYTHIA 6.228	`Cambridge`	Parton	10.409±0.022	8.838±0.020	0.849±0.002
JETSET 7.4	`Yclus`	Hadron	7.774±0.034	6.865±0.023	0.883±0.003
PYTHIA 6.228	`Yclus`	Hadron	7.846±0.012	7.066±0.011	0.901±0.001
PYTHIA 6.228	`Cambridge`	Hadron	7.443±0.019	6.273±0.017	0.843±0.002
DELPHI Data	`Cambridge`	Hadron	∼7.3	∼6.5	0.89±0.02
JETSET 7.4	`Yclus`	Track	8.110±0.035	7.376±0.024	0.909±0.003
PYTHIA 6.228	`Yclus`	Track	7.720±0.012	7.304±0.012	0.946±0.002
PYTHIA 6.228	`Cambridge`	Track	7.490±0.019	6.860±0.018	0.916±0.002
R17 Prod MC	`Yclus`	RecoTrk	8.122±0.036	7.547±0.025	0.929±0.003

Table 11: 4-jet rate for $b\overline{b}$ events and uds events. $y_{\rm cut}$ is 0.02 for JADE `Yclus` jet finder and 0.006 for `Cambridge` jet finder. All f_4 are actually $\geq$4 jet rates. All errors are for MC statistics only.

b quark mass. However, the physics picture behind that is much more than a single parameter of m_b. The gluon radiation, splitting, fragmentations, and b decays are happening at various different Q^2 so that the effective m_b are different depending on the process being examined. For the current version of the analysis we use the DELPHI measurement [26] of the ratio $R_4^{bl} = f_4(b\overline{b})/f_4(uds)$ in $b\overline{b}$ and uds events directly, where f_4 denotes the fraction of events are have $\geq$4 jets. The DELPHI paper was actually measuring exactly equal to 4 jets, but the $\geq$5 jet corrections is small enough, it doesn't make a significant difference compared to the DELPHI measuement error.

The DELPHI measurement of R_4^{bl} was performed for all final state hadrons using the `Cambridge` jet finder. We need to translate the result to corresponding bias for the JADE `Yclus` jet finder operating on charged tracks. To achieve this, we used the modern PYTHIA 6.228 [27] as the intermediate generator to relate the two sides. This also allows the verification of the various plots in [25] and [26] to ensure consistency. The DELPHI results are very stable against $y_{\rm cut}$ variations in the range 0.004 to 0.012 so we choose the $y_{\rm cut}$=0.006 point which gives absolute 4-jet rates fairly close to the JADE `Yclus` $y_{\rm cut}$=0.02 rates operating on tracks in our analysis. The 4-jet rates and ratios for various combinations of generators, particle levels and jet finders are listed in Table 11. For the particle input levels for the generator MC tests, results are tabulated for final partons (Parton), all final state stable particles (Hadron) and final state charged tracks (Track). The 4 jet rates in the R17 production MC with reconstructed tracks are alos included in Table 11 for completion. The R17 MC rates are for events after the hadronic selecton including $\cos\theta_{thrust}$ fiducial cut, but there are should be some track fiducial loss effects.

We construct scaling factors for the ratio bias (1-R_4^{bl}) based on the generator test results and DELPHI measurement listed in Table 11. The scaling factors are formed in two steps, using the PYTHIA 6.228 as an intermediate reference so that correction factors in each step are consistently extracted for the same jet finder and the same final state level.

The first step is to correct the JETSET 7.4 we used for MC production to the reference PYTHIA 6.228, using the results at the same final state level and same JADE `Yclus` jet finder:

$$S_J = \frac{1 - R_4^{bl}(\text{PYTHIA 6.228})}{1 - R_4^{bl}(\text{JETSET 7.4})}$$

This factor can be regarded mainly as a correction for the known excessive suppression for gluon radiation from heavy quarks in JETSET 7.4. However, as we have to make the connection of the `Yclus` finder results on tracks to the DELPHI `Cambridge` finder result on all hadrons, there is a caveat as to whether we should use the S_J correction derived from tracks or all hadrons. We will take the average of the two ways of calculating S_J and half of the difference between the two values as a systematic error to obtain $S_J = 0.72 \pm 0.13$.

The second step is to correct the PYTHIA 6.228 value toward the DELPHI data. This correction should be more representative of the subtle higher order effects such as effective running b quark mass which are not well controlled in the generators. For this correction we take the ratio between the DELPHI data and PYTHIA 6.228 using the all hadron level values using the `Cambridge` jet finder result as for the DELPHI measurement:

$$S_P = \frac{1 - R_4^{bl}(\text{DELPHI data})}{1 - R_4^{bl}(\text{PYTHIA 6.228})}$$

The R_4^{bl} distributions are rather flat as a function of y_{cut} for both DELPHI data and PYTHIA near the nominal y_{cut} region compared to the DELPHI data error. We obtain $S_P = 0.70 \pm 0.13$, with the uncertainty coming from the DELPHI measurement error.

Combining the two steps, we obtain an overall correction factor $S = S_J \cdot S_P = 0.50 \pm 0.13$. The bias due to 4-jet rate in the uncorrected R17 JETSET 7.4 MC is $\Delta R_b = 0.00117$, as in Table 10. Applying the correction factor S results in a corrected 4-jet rate bias of $\Delta R_b = 0.00059 \pm 0.00015$ for the R_b central value calculation.

As a crosscheck to verify the R_b event selection bias estimate for the 4-jet cut, we also performance analysis without the N_{jet} cut for the larger 97-98 data sample. One noticeable effect of the inclusion of the additional $\sim$10% of $\geq$4 jet events is that the overall b-tag correlation has changed by $\Delta C_b = +0.00383 \pm 0.00049$, where a major driver of the change is the larger fraction of events in the $\geq$4 jet sample with $2B$'s in the same hemisphere. Looking closely at just the additional $\geq$4 jet events alone, the MC indicate that the $g \to c\overline{c}$ and $g \to b\overline{b}$ event fractions are a factor of 4 and 10 respectively higher compared to the $\leq$3 jet events used for the nominal analysis. The R_b central value correction for scaling $g \to Q\overline{Q}$ from R17 MC to the LEPEWWG values has therefore changed from $\Delta R_b = -0.00150$ for the nominal analysis to -0.00185 for analysis without 4-jet cut. The additional complications in the tag correlations and extra sensitivity to $g \to Q\overline{Q}$ rates are the main reasons to exlcude these events from the nominal analysis. However, we have examined the various kinematic and vertexing quantities compared between data and MC for the additional $\geq$4 jet events alone and they are nonetheless still showing good agreement in general. Taking into account the $g \to Q\overline{Q}$ correction change, we find the difference in measured R_b due to the removal of $<$ 4-jet requirement is

$$R_b(\text{no } < 4 \text{ jet cut}) - R_b(\text{nominal analysis}) = +0.00042 \pm 0.00030 \pm 0.00015$$

Data period	93-95	96	97-98
Raw R_b measured	0.21626	0.21795	0.21913
Event selection bias	−0.00149	−0.00149	−0.00149
gamma/Z	+0.00030	+0.00030	+0.00030
$c\overline{c}$ prod/decay correction		+0.00015	+0.00012
$g \to Q\overline{Q}$ correction	−0.00046	−0.00139	−0.00150
tracking corrections		−0.00110	−0.00022
Scaling R_c to SM	−0.00004	−0.00004	−0.00004
Fully corrected R_b	0.21457	0.21438	0.21630

Table 12: Summary of central value corrections for the R_b measurement. The raw measurement refers to analysis using completely uncorrected MC, except published 93-95 raw value already included tracking corrections.

where the first error is the uncorrelated statistical uncertainty and second error is the systematic error on the estimated 4-jet cut bias. This is consistent with zero within statistics.

The total event selection bias for R_b is therefore $0.00149 \pm 0.00017_{MCstat} \pm 0.00015_{4-jet}$. The event selection bias for $c\overline{c}$ is consistent with zero and therefore no correction is applied for R_c. The R_b result central value corrections are summarized in Table 12.

5.5 Result stability checks

One possible source of systematic is poor modeling of the *uds* background that gives a secondary vertex due to badly reconstructed tracks. As a cross-check we tried to extract this effect from the data. We define a *uds* tag by requiring no secondary vertex and no track with a normalized 3D impact parameter of more than 2σ. This tag identifies about 50% of the *uds*, 15% of the *c* and 1.4% of the *b* hemispheres. Adding this tag to the other ones, we fit for the same efficiencies as before plus the ratio of *uds* giving a secondary vertex in data over Monte Carlo. We find a value of 1.1 ± 0.1 for this ratio.

We also examined the variation of the tagging efficiencies, the R_b result and the overall systematic errors as a function of the minimum y_{hem} cut for the *b* tag, over a wide range of y_{hem} cut, as shown in Fig. 30. The R_b result is stable within the 1σ total uncertainty envelope. We also examine in some detail on effect of the various R_b corrections on the central value, as shown in Fig. 31. The $g \to c\overline{c}$ correction is one the major sources of the slope, but some *D* decay systematics and tracking corrections can also be seen to be able to induce significant slope and wiggles. However, the sloping is confied at low y_{hem} and the result is stable at $y_{hem} > 0.75$ as we hoped.

6 Conclusions

We have measured the hadronic branching ratio of the Z^0 to *b* quark and *c* quark with our 96-98 dataset of ∼400,000 hadronic Z^0 decays. The 96 and 97-98 results are combined,

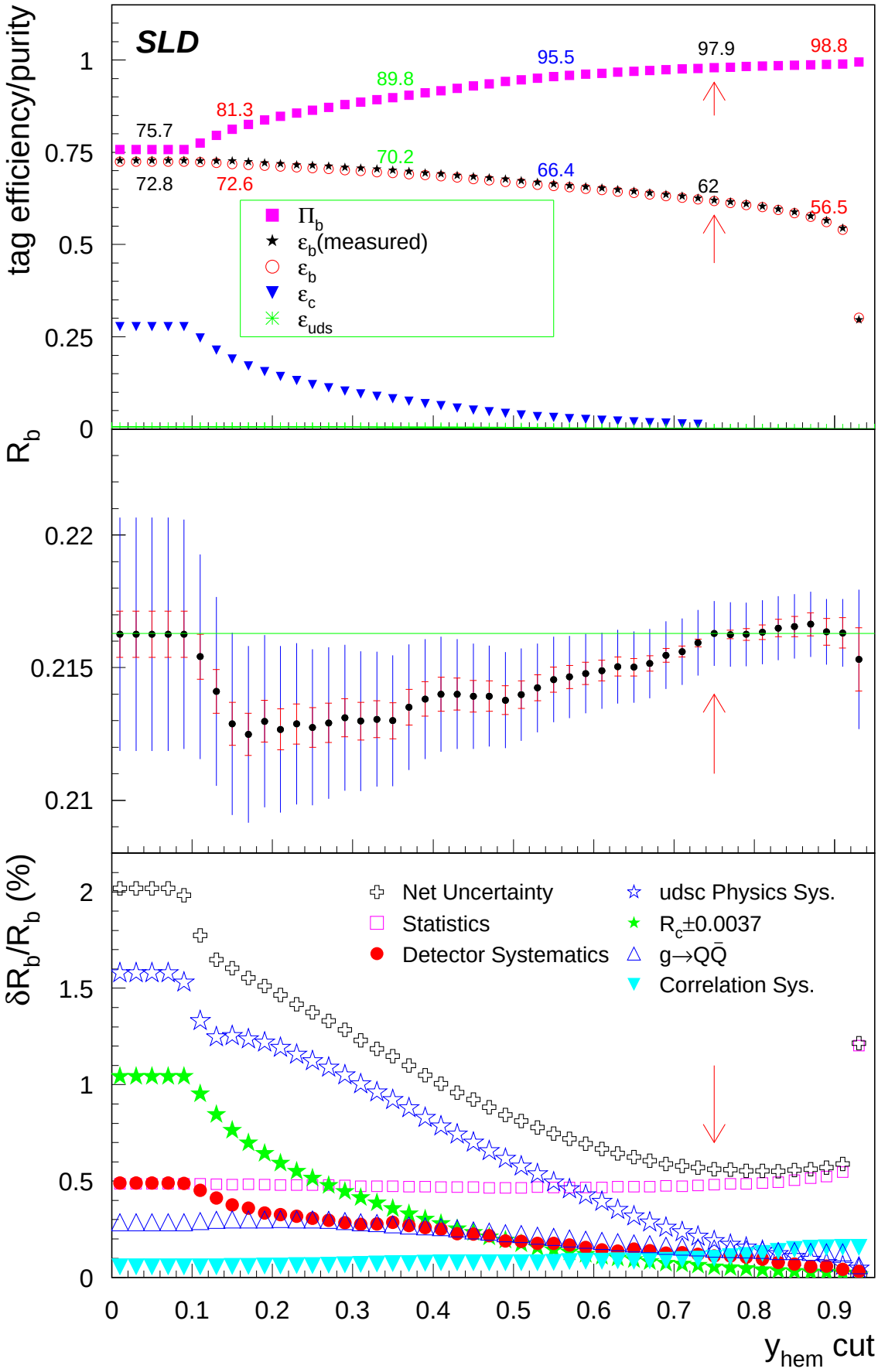

Figure 30: a) Tagging efficiencies and b purity. b) variation of the measured value of R_b, with the inner error bar being uncorrelated statistical error w.r.t. the nominal cut and the total error. c) R_b statstical and systematic error components as a function of the b-tag selection cut, for 97-8 analysis. The net uncertainty does not yet include event selection uncertainties.

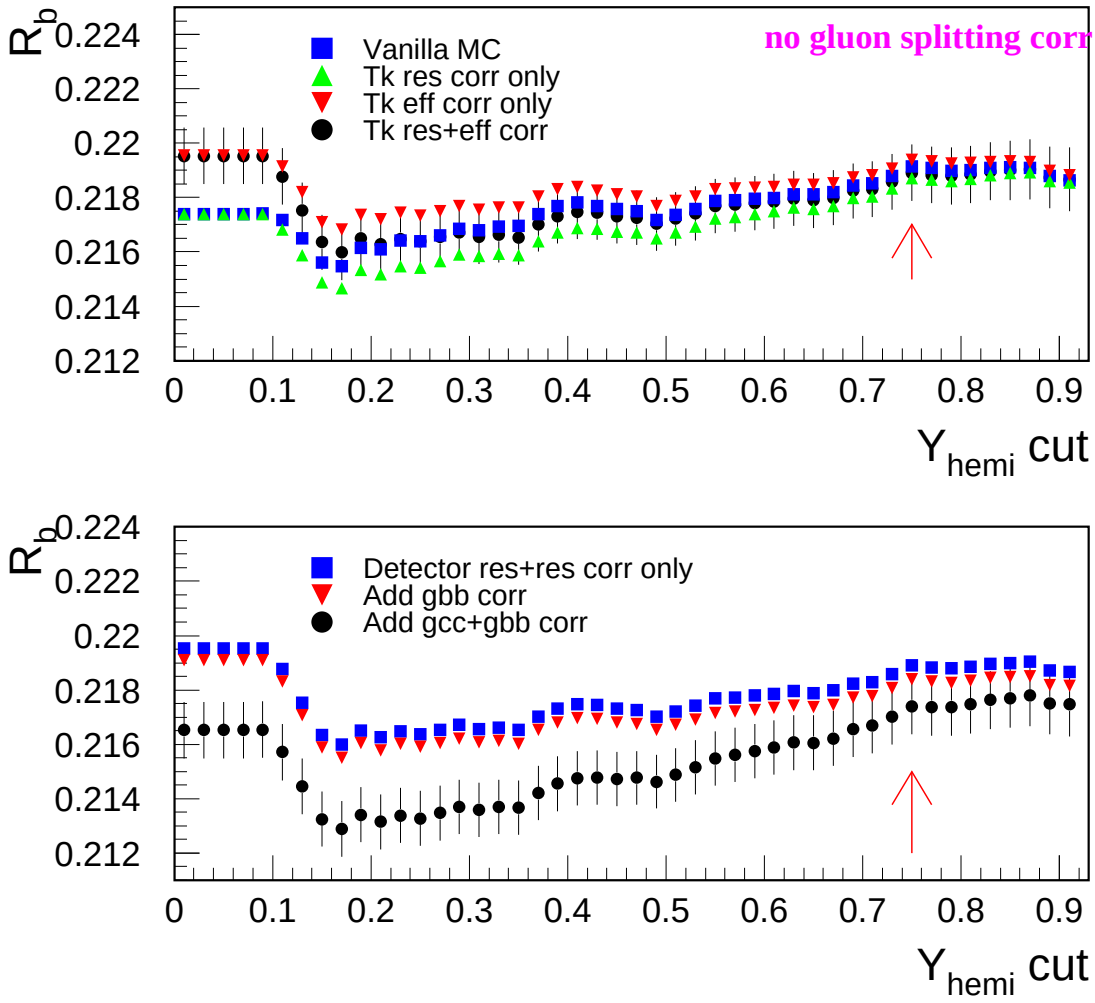

Figure 31: Variation of the measured value of R_b as a function of the b-tag selection cut at various stages of central values corrections, for 97-8 analysis.

with all common systematic uncertainties, including detector uncertainties, treated as fully correlated. The combined results are:

$$\begin{array}{lcllll} R_b & = & 0.21610 & \pm 0.00098(\text{stat}) & \pm 0.00073(\text{sys}) & \mp 0.00012(R_c) \\ R_c & = & 0.1745 & \pm 0.0031(\text{stat}) & \pm 0.0020(\text{sys}) & \mp 0.0006(R_b) \end{array}$$

For the R_b measurement, combining this new measurement with our previously published result on the 93-95 data [2], we obtain:

$$R_b = 0.21600 \pm 0.00094(\text{stat}) \pm 0.00074(\text{sys}) \mp 0.00012(R_c)$$

The relative weights in the combined average for the 93-95:96:97-98 (96:97-98) R_b (R_c) measurements are 7:9:84 (11:89), dominated by the 97-98 result. These measurements are in good agreement with the Standard Model expectation of R_b=0.2157 (for m_t=178 GeV/c^2) and R_c=0.1723. They can be compared with the average of LEP measurements [28] from a total of ∼16 M hadronic Z^0 decays:

$$\begin{array}{lcllll} R_b & = & 0.21643 & \pm & 0.00073 \\ R_c & = & 0.1691 & \pm & 0.0047 \end{array}$$

In conclusion, we have exploited the high resolution vertexing capability and the small and the stable SLC IP for a precision test of Standard Model through the measurements of heavy quark production fractions in Z^0 decays. Our new R_c result is by itself more precise than the current world average [18]. These measurements confirm the Standard Model predictions at ∼0.6% precision for R_b and 2.1% precision for R_c.

We thank the staff of the SLAC accelerator department for their outstanding efforts on our behalf. This work was supported by the U.S. Department of Energy and National Science Foundation, the UK Particle Physics and Astronomy Research Council, the Istituto Nazionale di Fisica Nucleare of Italy and the Japan-US Cooperative Research Project on High Energy Physics.

References

[1] ALEPH Collab, R. Barate *et al.*, Phys. Lett. **B 401** (1997) 150.
ALEPH Collab, R. Barate *et al.*, Phys. Lett. **B 401** (1997) 163.
DELPHI Collab, P. Abreu *et al.*, Eur. Phys. J **C10** (1999) 415.
L3 Collab, M. Acciari *et al.*, Eur. Phys. J **C13** (2000) 47.
OPAL Collab, G. Abbiendi *et al.*, Eur. Phys. J **C8** (1999) 217.

[2] SLD Collab., K. Abe *et al.*, Phys. Rev. Lett. **80** (1998) 660.

[3] ALEPH Collab, R. Barate *et al.*, Eur. Phys. J **C4** (1998) 557.
DELPHI Collab, P. Abreu *et al.*, Eur. Phys. J **C12** (2000) 209.
DELPHI Collab, P. Abreu *et al.*, Eur. Phys. J **C12** (2000) 225.

OPAL Collab, K. Ackerstaff *et al.*, Eur. Phys. J **C1** (1998) 439.
ALEPH Collab, R. Barate *et al.*, Eur. Phys. J **C16** (2000) 597.
OPAL Collab, G. Alexander *et al.*, Z. Phys. J **C72** (1996) 1.

[4] M. Breidenbach, IEEE Trans. Nucl. Sci. **33** (1986) 46.

[5] SLD Collaboration, K. Abe *et al.*, Phys. Rev. **D53** (1996) 1023.

[6] M.D. Hildreth *et al.*, IEEE Trans. Nucl. Sci. **42** (1994) 451.

[7] K. Abe *et al.*, Nucl. Instr. Meth. **A400** (1997) 287.

[8] D. Axen *et al.*, Nucl. Inst. Meth. **A328** (1993) 472.

[9] D. J. Jackson, D. Su and F.J. Wickens, Nucl. Inst. and Meth. **A510**, 233 (2003).

[10] T. Sjöstrand, Comput. Phys. Commun. **82** (1994) 74.

[11] P. N. Burrows, Z. Phys. **C41** (1988) 375.
OPAL Collab., M.Z. Akrawy *et al.*, Z. Phys. **C47** (1990) 505.

[12] R. Brun *et al.*, Report No. CERN-DD/EE/84-1 (1989).

[13] A. S. Chou, Ph.D thesis, Stanford Univ., SLAC-R-578 (2001).

[14] JADE Collab., W. Bartel *et al.*, Z. Phys. **C33** (1986) 23.

[15] D. J. Jackson, Nucl. Inst. and Meth. **A388**, 247 (1997).

[16] T. R. Wright, Ph.D thesis, U. of Wisconsin, SLAC-R-602 (2002).

[17] The LEP Electroweak Working Group, D. Abbaneo *et al.*, LEPHF/2001-01 (November 2001).

[18] S. Eidelman *et al.*, Phys. Lett. B **592**, 1 (2004).

[19] C. Peterson, D. Schlatter, I. Schmitt and P.M. Zerwas, Phys. Rev. **D27** (1983) 105.

[20] M.G. Bowler, Z. Phys. **C11** (1981) 169.

[21] D. Coffman *et al.*, Phys. Lett.**B263** (1991) 135.

[22] G. Marchesini *et al.*, Comp. Phys. Comm. **67** (1992) 465.

[23] S.E Walston, Ph.D thesis, U. of Oregon, SLAC-R-728 (2004).

[24] DELPHI Collab.: P. Abreu *et al.*, Phys. Lett. **B418** (1998), 430; A. Brandenburg, P. Burrows, D. Muller, N. Oishi and P. Uwer, Phys. Lett. **B468** (1999), 168; ALEPH Collab.: R. Barate *et al.*, Eur. Phys. J **C18** (2000) 1; OPAL Collab.: G. Abbiendi *et al.*, Eur. Phys. J **C21** (2001) 411.

[25] E. Norrbin and T. Sjöstrand, Nucl. Phys. **B603** (2001), 297.

[26] DELPHI Collab.: P. Bambade *et al.*, Contributed paper 5-0139, ICHEP-04, Aug 2004, Beijing, China; DELPHI 2003-023 CONF 642 (2003). Publication in preparation.

[27] T. Sjöstrand *et al.*, Comp. Phys. Comm. **135** (2001) 238, hep-ph/0108264 (2001).

[28] The LEP Collaborations, the LEP Electroweak Working Group and the SLD Electroweak and Heavy Flavor Working Groups, CERN-PH-EP/2004-069, hep-ex/0412015, Dec/2004.

	$\delta R_b(10^{-5})$	$\delta R_c(10^{-5})$
MC statistics	13	91
$g \to b\overline{b}$ 0.254±0.051%	-24	9
$g \to c\overline{c}$ 2.96±0.38%	-23	-101
long lived light hadron production ±10%	-1	-1
D^+ production 0.259 ± 0.028	-10	-6
D_s production 0.115 ± 0.037	-11	-15
c-baryon production 0.074 ± 0.029	-11	22
charm fragmentation	-18	18
D^0 lifetime 0.415 ± 0.004 ps	-3	8
D^+ lifetime 1.057 ± 0.015 ps	-2	5
D_s lifetime 0.467 ± 0.017 ps	-3	-3
Λ_c lifetime 0.206 ± 0.012 ps	-1	-91
D decay multiplicity	-27	60
D decay K^0	19	56
D decay no-π^0	-9	12
B lifetime ±0.05 ps	0	5
B decay $\langle N_{ch} \rangle = 5.73 \pm 0.35$	-20	3
b fragmentation	4	26
Λ_b production fraction 0.074 ± 0.030	5	-2
QCD hemisphere correlation	6	22
hard gluon radiation	-2	26
tag geometry dependency	9	17
tag time dependency	1	1
component correlation	14	45
tracking resolution	27	22
tracking efficiency	13	3
$\langle IP \rangle_{xy}$ tail	2	0
event selection bias	17	20
4 jet rate in b events	15	0
$R_c = 0.1723 \pm 0.0037$	-12	
$R_b = 0.2157 \pm 0.0010$		-62
Total (excl. $R_{b/c}$)	**73**	**200**

Table 13: Summary of systematic uncertainties for R_b and R_c.
A $-$ sign for an error means the value for R_q goes down when this parameter is varied upward. The errors are assumed to be symmetric.